REVIEW

Check for updates

Surface-enhanced Raman spectroscopy as a tool for food and environmental monitoring of pesticides: recent trends and perspectives

Gabriel Fernandes Souza dos Santos, [ID] [a] Giordano Toscano Paganoto, [ID] [a] Lucas Carreira Cosme, [ID] [a] Adilson Ribeiro Prado,[b] Sérvio Túlio Alves Cassini,[c] Marco César Cunegundes Guimarães[a] and Jairo Pinto de Oliveira [ID] *[a]

Surface-enhanced Raman spectroscopy (SERS) has emerged as a powerful analytical tool for ultrasensitive detection of environmental contaminants, particularly pesticides. Recent developments have focused on nanomaterials engineering and SERS-active sensors to enhance signal intensity. Gold (AuNPs) and silver nanoparticles (AgNPs) of various morphologies and sizes have been widely explored due to their plasmonic properties, as well as hybrid or combined nanoparticle systems. Innovative approaches have also been developed, such as embedding nanoparticles in gels to enhance stability and reproducibility or using magnetic nanoparticles for sample interaction and preconcentration. Additionally, the integration of graphene oxide has gained attention because of its ability to improve the chemical enhancement mechanism *via* $\pi-\pi$ interactions with analyte molecules. Despite these advances, SERS-based detection remains challenging, particularly with regard to selectivity in complex matrices. To address this issue, recent strategies have combined SERS substrates with biorecognition molecules such as antibodies, aptamers, and enzymes, thereby improving specificity and facilitating the development of SERS-based biosensors. This review highlights the current state-of-the-art SERS applications for pesticide detection

[a]*Federal, University of Espírito Santo (Ufes), Campus Maruípe, 29047-105 Vitória – ES, Brazil. E-mail: jairo.oliveira@ufes.br*

[b]*Federal Institute of Espírito Santo (Ifes), Campus Serra, Serra – ES, 29166-630, Brazil*

[c]*Federal University of Espírito Santo (Ufes), Campus Goiabeiras, Vitória – ES, 29075-910, Brazil*

Gabriel Fernandes Souza dos Santos is a postdoctoral researcher at the Environmental Characterization Laboratory (Lacar-UFES) and the Functional Nanomaterials Laboratory (LNF-UFES). He holds a BSc, MSc, and PhD in Chemistry from the Federal University of Espírito Santo. Dos Santos has expertise in analytical method development, electroanalytical chemistry, nanomaterials, multifunctional materials, green chemistry, and food analysis. He has published over 20 peer-reviewed articles in high-impact journals and currently focuses on developing multiplex Raman spectroscopy platforms for sensitive and selective pesticide detection, integrating advanced nanostructured substrates with analytical innovation.

Gabriel Fernandes Souza dos Santos

Giordano Toscano Paganoto received his bachelor's degree in chemistry from the Federal University of Viçosa in 2013. He obtained his master's degree in 2016 at the Federal University of Espírito Santo. In 2022, he received his PhD degree under the supervision of Prof. Dr Márcia Temperini at São Paulo University, specializing in Surface-Enhanced Raman Spectroscopy (SERS) and plasmonic nanostructures. He is currently working as a postdoctoral researcher under the supervision of Prof. Jairo Pinto at the Federal University of Espírito Santo. His research is mainly focused on the development of SERS-based sensors for pesticide detection and LFIA.

Giordano Toscano Paganoto

in food and environmental samples, discussing the key technological advances, material innovations, and analytical challenges. This paper also offers perspectives on future research directions to increase the sensitivity, reproducibility, and field applicability of SERS-based detection platforms.

1. Introduction

Maintaining global food production and security has become a significant issue in the current era. According to the State of Food Security and Nutrition in the World 2023 report by the Food and Agriculture Organization (FAO), an estimated 691 million to 783 million people worldwide faced hunger in 2022. To put this into perspective, approximately 735 million individuals fell within the midrange estimate, representing an alarming increase of 122 million people experiencing hunger in 2022 compared to the pre-pandemic year of 2019.[1] However, if not well managed, large-scale food production could present global public health risks, as evidenced by periodic zoonotic foodborne disease outbreaks worldwide. These outbreaks have diverse causes, including interactions between humans and animals, inadequate infrastructure, and suboptimal post-harvest practices, leading to food contamination by viruses, bacteria, parasites, and prions. Another major problem is the utilization of several chemicals, including toxins, industrial compounds, heavy metals, persistent organic pollutants, and pesticides, which lead to various health-related issues.[2–4]

Concerns regarding pesticide use are complex and involve environmental, health, and regulatory aspects.[5–7] Pesticides are extensively used in regions with intensive agriculture and have elicited concerns regarding their potential ecological consequences.[2] These chemicals linger in the environment, contaminate soil and water, and pose risks to nontarget organisms and ecosystems.[5] Health concerns arise as pesticide residues enter the food chain and threaten human health.[6] Most pesticides are mainly grouped as organochlorines, carbamates, triazines, and organophosphates, like glyphosate, which is the most widely used in current agriculture.[8,9] Glyphosate can display endocrine-disrupting activity, promote carcinogenicity in mouse skin, and affect human erythrocytes. Triazines, such as atrazine, are related to endocrine-disrupting effects and reproductive toxicity, and are potentially related to breast cancer.[10] Balancing high agricultural productivity while minimizing unintended consequences is a significant challenge that requires ongoing research, innovative approaches, and global cooperation to obtain comprehensive solutions.[11] In addition, establishing and adhering to maximum residue limits (MRLs) highlight the need for strict regulatory frameworks. In addition, reliance on advanced external laboratories for pesticide analysis introduces challenges that affect market activities and decision-making processes.[2]

The most traditional analytical methods for pesticide detection involve gas chromatography (GC) and high-performance liquid chromatography (HPLC) as separation techniques and mass spectrometry (MS) as the detection technique.[12,13] Several experimental protocols based on solvent extraction, solid-phase extraction, and other methods have been developed to improve pesticide detection.[14,15] However, these traditional methods use several organic solvents, sample preparation, time-consuming analysis, and a skilled operator.[12–16]

Surface-Enhanced Raman Spectroscopy (SERS) is emerging as a novel approach to advancing pesticide detection in food and environmental matrices.[17] SERS can amplify the Raman signal through local electric field enhancement (EM) by exciting surface plasmon resonance (SPR) in plasmonic nanomaterials like gold (AuNPs) and silver (AgNPs) nanoparticles.[18–20] Another

Lucas Carreira Cosme

Lucas Carreira Cosme is a Biomedical Sciences student (6th semester) at IFES. He has volunteered as a laboratory assistant at the Translational Pharmacology and Physiology Laboratory at UVV, and in the Protein and Microbiology Laboratories at UFES. He is an active member of the IFES Academic Pathology League and serves as a teaching assistant for Health Analysis Techniques. Cosme conducts undergraduate research on the synthesis of gold nanoparticles for SERS multiplex pesticide detection and participates in a voluntary project investigating in vitro and in silico chalcone derivatives with potential anti-Helicobacter pylori, anti-inflammatory, and antitumor activities.

Jairo Pinto de Oliveira

Jairo Pinto de Oliveira received his PhD in Biotechnology from the Federal University of Espírito Santo (UFES), Brazil, and completed a postdoctoral fellowship in Nanosensors at the Physics Institute of São Carlos (USP). Currently, he is a professor at UFES and serves as the coordinator of the Functional Nanomaterials Laboratory. Oliveira's research interests include bio- and nano-sensors, nanomaterials, plasmonics, LSPR, SPR, Raman spectroscopy, paper-based devices, and optical characterization. He has published over 60 peer-reviewed papers in reputable international journals. Additionally, he serves as a regular reviewer for several high-impact journals, including Nanoscale, Talanta, Chemistry of Materials, Analytical Chemistry, ACS Sensors and Advanced Materials.

enhancement mechanism that can increase the Raman signal is the chemical enhancement mechanism (CM) due to the electronic coupling (charge transfer mechanisms) of molecules adsorbed (or chemisorption) on roughened metal surfaces.[21] Both mechanisms increase the intensity of the Raman signal (enhancement factor, EF) by 10^4 to 10^{10}-fold, which enables the quantification of target compounds at trace concentrations.

To successfully detect chemical analytes using SERS measurements, some requirements need to be met: (i) a suitable substrate must have a roughened surface or controllable particle size to provide good enhancements and reproducibility; (ii) it must be robust with a long lifetime; (iii) the analyte must adsorb or strongly interact with the substrate surface; (iv) for accurate quantitative measurements, it is preferable to average multiple events by regulating the number of active sites within the interrogation volume and controlling the interrogation duration; (v) to obtain reliable quantitative SERS measurements, using a standard is ideal for tracking variations caused by substrate changes.[22–25]

Numerous review articles have demonstrated significant advancements in this field, focusing on enhancing the SERS signals to achieve lower detection limits.[22,26–32] These studies explored various shapes and sizes of plasmonic nanoparticles and different combinations with non-plasmonic materials to produce SERS sensors for pesticide analysis. However, most of these reviews do not focus exclusively on pesticide detection and typically center on a single type of substrate or nanomaterial, limiting their scope in addressing the broader challenges specific to pesticide analysis.[29,33]

One of the notable applications of SERS is to significantly improve the effectiveness of other methods, such as lateral flow immunochromatographic assays (LFA). LFAs are well-known for their affordability, simplicity, and rapid detection ability, and they are commonly applied in clinical testing.[34] Although the trends and progress in LFA technology have been reviewed by Jara *et al.* (2022) and Zhang *et al.* (2021), the use of SERS in these assays still needs to be explored.[35,36] The combination of LFA with SERS (LFA-SERS) offers a simple yet powerful method that provides both qualitative and quantitative information and emphasizes the use of antibodies or aptamers to enhance the method's selectivity.

In this context, this review presents an overview of the current state of SERS applications for monitoring pesticides in food and environmental matrices. This study provides a global overview of pesticide usage, SERS principles and formats, substrate types, and a detailed survey of existing SERS strategies for pesticide detection. In addition, the review discusses the significant advancements and challenges faced and outlines future perspectives for the continued use of these devices in monitoring pesticides in the environment. Despite these advancements, more detailed reviews in the literature regarding innovative approaches using SERS are still needed. This study aims to fill this gap by reviewing the use and theory of SERS for pesticide detection, highlighting the role of graphene and semiconductor metals, and exploring the potential of LFA-SERS for improved selectivity and quantification. In addition, new approaches involving plasmonic materials, Raman labels, magnetic particles, and biorecognition are discussed.

2. Mechanisms of SERS enhancement

SERS is a powerful analytical technique capable of detecting molecular species at extremely low concentrations, including the single-molecule level. First observed by Fleischmann *et al.* in 1974 while studying the pyridine adsorption on a roughened silver electrode,[37] SERS was later correctly interpreted by Jeanmaire and Van Duyne,[38] and by Albrecht and Creighton,[39] who demonstrated that the enhancement of the Raman signal was not merely due to increased surface area but resulted from a significant amplification of the Raman scattering cross-section. In 1978, Moskovits proposed that this effect originated from the excitation of surface plasmons on rough metal surfaces,[40] which led to a systematic understanding of enhancement mechanisms and the prediction that metals like silver, gold, and copper would be especially effective SERS substrates. Nowadays, it is well established that the SERS effect can be interpreted by two main mechanisms: electromagnetic mechanism (EM) and chemical mechanism (CM).

2.1 Electromagnetic mechanism

The EM mechanism is widely recognized as a dominant contributor to the SERS effect. This mechanism relies on the amplification of the local electromagnetic field near metallic nanostructures due to the excitation of LSPR.[41–44] These plasmonic excitations create intense local electromagnetic fields near the metal surface. When light interacts with a metallic nanoparticle much smaller than the incident wavelength, the conduction electrons in the metal oscillate collectively, forming a localized plasmon[45,46] (Fig. 1).

At resonance, this induces a depolarization field that cancels the external field, resulting in substantial local electric field enhancement.[47] This resonance condition is satisfied when the real part (Re) of the nanoparticle's complex dielectric function (ε) is $\mathrm{Re}(\varepsilon) = -2\varepsilon_\mathrm{m}$, where ε_m is the dielectric constant of the surrounding medium and the $\mathrm{Im}(\varepsilon)$ is small, according to the real part and imaginary parts for different metals (Fig. 2). It is worth mentioning that the coinage metals (Au, Ag, and Cu) exhibit this resonance condition at visible wavelengths, where most of the Raman experiments are conducted.[48,49]

The theoretical basis of the EM mechanism relies on the classical treatment of Raman polarizability, which modulates the strength of the induced Raman dipole moment in response to the incident electromagnetic field.[50] When a molecule is adsorbed onto or located in the vicinity of a metallic nanostructure, both the Raman polarizability and the local field can be significantly altered by the metallic object. The emission of any dipole near the surface is also modified, which affects the SERS intensity, leading to an EF given by:[51]

$$\mathrm{EF} = \frac{|E_\mathrm{loc}(\omega_\mathrm{L})|^2}{|E_0|^2} \frac{|E_\mathrm{loc}(\omega_\mathrm{R})|^2}{|E_0|^2} \tag{1}$$
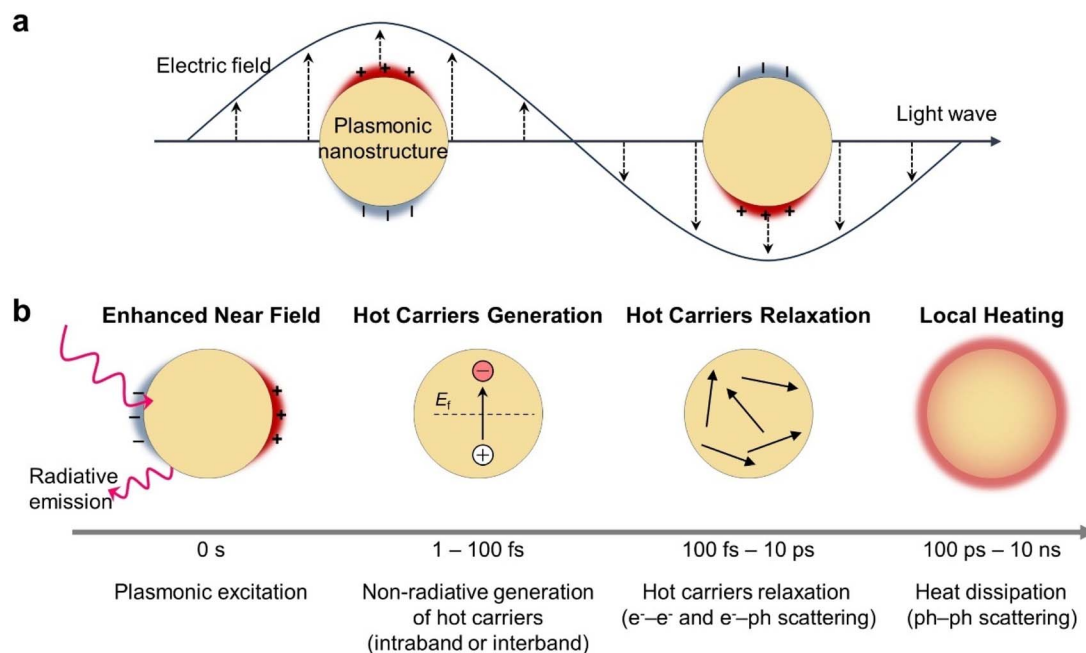
Fig. 1 Plasmonic excitation and decay in plasmonic nanostructures: (a) plasmonic excitation by irradiation. (b) Decay through radiative photon emission or non-radiative generation of hot carriers followed by relaxation through electron–electron and electron–phonon scattering, and ending with heat dissipation through phonon scattering. This figure has been adapted/reproduced from ref. 46 with permission from Willey, copyright 2025.
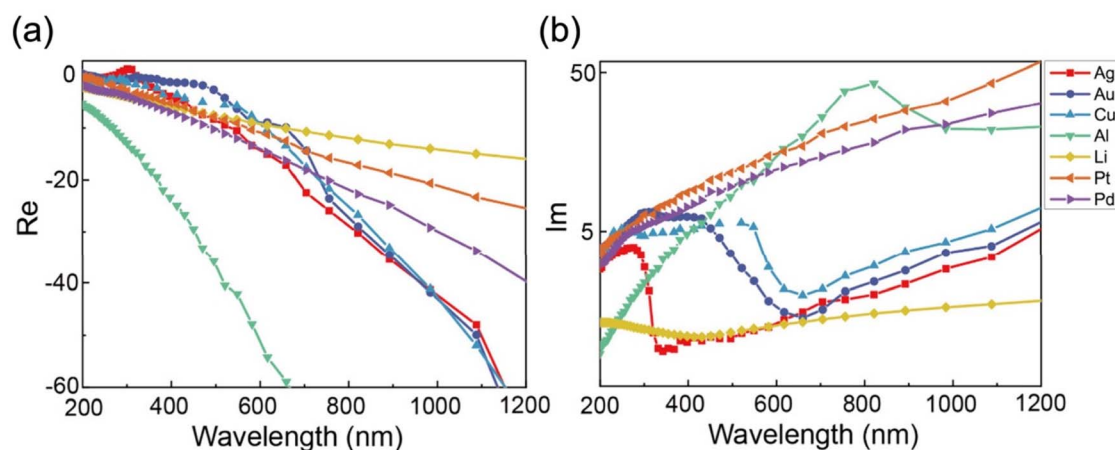

Fig. 2 (a) Real (Re) and (b) imaginary (Im) parts of the dielectric function of different bulk metals. This figure has been adapted/reproduced from ref. 49 with permission from American Chemical Society, copyright 2025.

Here, $E_{\text{loc}}(\omega_{\text{L}})$ and $E_{\text{loc}}(\omega_{\text{R}})$ are the amplitudes of the local electric field at the excitation (ω_{L}) and Raman emission (ω_{R}) frequencies, respectively, while E_0 is the amplitude of the incident electric field. Note that the ratio $|E|/|E_0|$ indicates that the EF does not depend on the incident laser power.

$$\frac{|E_{\text{loc}}(\omega_{\text{L}})|^2}{|E_0|^2} \approx \frac{|E_{\text{loc}}(\omega_{\text{R}})|^2}{|E_0|^2} \quad (2)$$

In this sense, the EF could be expressed in terms of the fourth power of the local electric field.[50]

$$\text{EF} = \left(\frac{|E_{\text{loc}}(\omega_{\text{L}})|}{|E_0|}\right)^4 \quad (3)$$

Although this approximation slightly overestimates the enhancement for isolated homogeneous particles, it remains widely used due to its practicality.[41,42] For low-frequency Raman modes, the enhancement can scale approximately with the fourth power of the local field strength, leading to signal increases by factors of 10^4 to 10^6 or higher.[40]

2.1.1. SERS enhancement factors. The previous definition of SERS EF (eqn (3)) represents a theoretical approximation that considers only a molecule located at a well-defined position on a metallic surface. In practical SERS experiments, there are many molecules located at different positions on the surface (or nearby) where the field enhancement can differ significantly, which is further magnified by the fourth power dependence. Most SERS substrates present a wide distribution of EF, with the maximum EF differing from the minimum EF by several orders of magnitude. It is well established that the regions of maximum EF, called hot spots, dominate the SERS signal. For most SERS substrates, a pragmatic way to estimate the EF based only on the concentration and SERS intensity of an analyte is to define the analytical enhancement factor as:

$$AEF = \frac{I_{SERS}/C_{SERS}}{I_{Raman}/C_{Raman}} \qquad (4)$$

where C_{SERS} and C_{Raman} are the analyte concentrations used in preparation, and I_{SERS} and I_{Raman} are the respective analyte intensities under SERS and Raman conditions. It is important to mention that other enhancement factors could be estimated;[52] however, eqn (4) presents a practical and straightforward way to calculate the EF. Although the AEF strongly depends on the type of analyte, the adsorption efficiency does not consider the CM; it is widely used to estimate the EF for SERS substrates and pesticides such as thiram,[53] diuron,[54] atrazine[54] and others.[55–57]

2.1.2. Engineering electromagnetic enhancement. Engineering electromagnetic enhancement in SERS relies on the strategic design of metallic nanostructures to maximize LSPR, which intensifies the Raman signal by concentrating the electromagnetic field in nanoscale regions called hot spots.[58] These hot spots are strongly influenced by the geometry, size, composition, spatial arrangement, and dielectric environment of the nanostructures.[58–61]

Nanoparticles with sharp or anisotropic features, such as nanostars, nanocubes, and nanoprisms, are especially effective at producing high field intensities. The electric field tends to concentrate at tips, edges, and corners, enhancing the Raman signal of nearby molecules through the lightning rod effect.[41] Core–shell structures and tightly coupled dimers also support intense hot spots within nanogaps. These configurations benefit from strong plasmonic coupling, which can be tuned by controlling interparticle spacing or shell thickness using self-assembly techniques, chemical linkers, or templated synthesis.[27,62,63]

Laser polarization and particle orientation also affect enhancement. For example, in nanowire–nanoparticle junctions, SERS intensity varies with the direction of polarization relative to the wire axis.[64] Remote excitation strategies using metallic nanowires can deliver plasmons over long distances, generating localized Raman signals at specific junctions.[65,66] This approach reduces background noise and allows localized detection with high sensitivity.[24]

Fabrication methods play a crucial role in determining both enhancement and reproducibility. Bottom–up approaches, such as solvent evaporation, allow the formation of dense nanoparticle aggregates with narrow nanogaps.[67] Top–down techniques, including nanoimprint lithography, colloidal lithography, and block copolymer templating, enable precise control of nanostructure size and periodicity.[67,68] These substrates offer consistent enhancement across large areas and are compatible with scalable manufacturing.

The size of the nanostructures is also a determining factor. SERS activity is typically strongest for nanoparticles between 20 and 70 nanometers, where LSPR efficiently matches the excitation wavelength while maintaining strong polarizability.[62,69,70] For elongated structures like nanorods, aspect ratio tuning enables resonance splitting into longitudinal and transverse modes. Shape also influences plasmon behavior. For instance, nanoprisms and nanocrescents can support multiple plasmon modes, while sharp structures improve enhancement through better field localization.[62,69,70]

The selection of material further affects performance. Silver provides the highest enhancement in the visible range but is chemically unstable, whereas gold offers better biocompatibility and long-term stability.[71,72] Hybrid nanostructures and protective coatings such as silica or graphene can combine stability with high enhancement, maintaining performance in complex environments.[71,72] Simulations have shown that geometries like hemi-spheroids, nanocones, and nanoshells can be tailored for specific wavelengths and enhancement levels by adjusting parameters such as eccentricity and particle separation.[71,72]

In summary, electromagnetic enhancement in SERS can be finely engineered through the rational design of nanostructures, guided by both experimental fabrication and computational modeling. Optimization of geometry, material, and assembly techniques is essential for achieving high enhancement factors, reproducible performance, and application versatility.

2.2 Chemical enhancement mechanism

Despite the EM mechanism being dominant for the SERS effect, it does not consider any aspects related to the tensorial nature of the Raman polarizability, the orientation of the molecules, and changes in molecular properties. The chemical enhancement can be classified as resonance Raman enhancement, photoinduced charge-transfer resonance from the substrate to the molecule or *vice versa*, and adsorption-induced changes in polarizability (mainly for non-resonant molecules).[49]

The fundamental steps of the CM are illustrated in Fig. 3A. This mechanism proposes that adsorption of the molecule on the metallic surface forms a surface complex that modifies the polarizability tensor, compared to the free molecule. The primary steps involve the Herzberg–Teller vibronic coupling between the metal and the adsorbed molecule, with the coupling terms, h_{F-K} and h_{I-F} (red arrows in Fig. 3A).[73] As a consequence, the gap between the HOMO and LUMO is reduced and the resonance for the charge transfer moment (μ_{CT}), borrowed from the molecular transition μ_{I-K}, can be activated at a lower energy than needed for a free molecule. A photoinduced electron can be excited either from the HOMO to
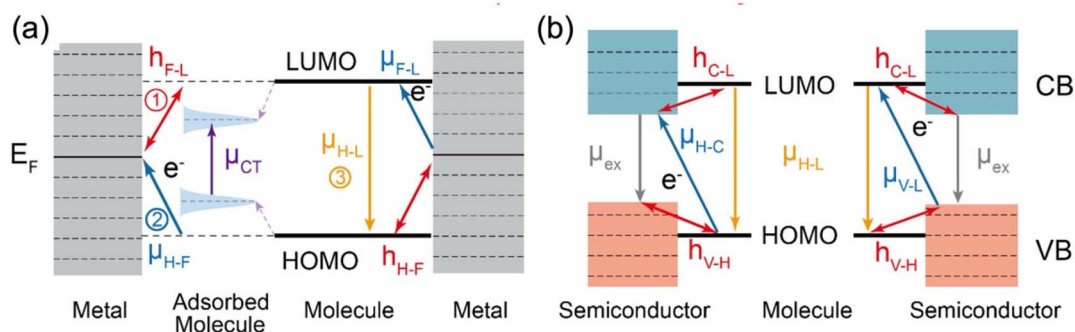
Fig. 3 Charge transfer pathways: (a) metal–molecule and (b) semiconductor–molecule. This figure has been adapted/reproduced from ref. 49 with permission from American Chemical Society, copyright 2025.

the metal Fermi level *via* the molecule-to-metal transition moment μ_{HF} through energy h_{F-L}, or from the Fermi level to the molecule LUMO *via* the metal-to-molecule transition moment (μ_{F-L}) through energy h_{HF} (blue arrows in Fig. 3A). Finally, the electrons relax back to the HOMO, emitting a Raman photon that carries fingerprint information about the adsorbed molecule.[49,74]

As mentioned, CT enhancement can occur in both resonant and non-resonant regimes. In the non-resonant case, the enhancement is relatively modest (typically 10–100×), yet significant even in the absence of electromagnetic hot-spots.[45,62,70] In contrast, CT resonance described through vibronic coupling models can lead to much larger enhancements. Importantly, recent advances in density functional theory (DFT) have enabled quantitative prediction of these CT interactions and their effect on Raman intensities.[45,62,70,75,76]

Recent DFT studies have reinforced the role of CM by analyzing benzenethiol derivatives adsorbed onto silver clusters (Ag_{19}).[50] These studies demonstrate that variations in enhancement factors are closely linked to the nature and position of functional groups, particularly *via* inductive and mesomeric effects that influence charge-transfer interactions with the metal. *Meta*-substitution shows a smoother trend aligned with halogen electronegativity, while *para*-substitution engages more complex π-electron interactions. These findings support that CM is governed by molecular electronic structure and its coupling to the metal surface. Additionally, solvation was shown to increase the CM effect, indicating that solvent polarity can enhance metal-molecule charge-transfer efficiency.[50,77]

2.2.1. Charge transfer mechanism for semiconductors. Plasmonic materials have plenty of free electrons capable of supporting LSPR phenomena in the visible region; this is not the case for semiconductor materials. The much lower free charge carrier density makes it a difficult task to bring the LSPR frequency into the visible light region. Even with several modifications and tuning strategies, the LSPR frequency of doped semiconductors can only be tuned to the near-infrared light region, far from the common wavelength used in Raman spectroscopy.[78–80] In this sense, it is acceptable that the CM and photoinduced charge transfer PICT process plays a crucial role in SERS on semiconductor platforms.

To realize the CT process in a semiconductor SERS active substrate it is essential to consider some aspects to simplify understanding: (i) only the electrons of occupied orbitals can be transferred to other energy levels; thus occupied orbitals like the HOMO and the valence band (VB) of the semiconductor can act as electron donors; (ii) only unoccupied orbitals like the LUMO and the conduction band (CB) of the semiconductor can act as electron acceptors; (iii) as a resonance-like process the CT involves either molecular transition (resonance Raman) or exciton transition (resonance of semiconductors); thus the CT pathways are combinations or arrangements of the donors and acceptors mentioned earlier, resulting in various CT transition moments.[49,79,81] The VB and CB can function similarly to the Fermi level in SERS enhancement, which stems from intensity borrowing *via* the allowed molecular transition μ_{H-L} (blue arrows in Fig. 3b) with four representative CT Herzberg–Teller coupling processes, as follows:[78,82]

(1) HOMO to CB: photoinduced electron transfer from the molecular HOMO to the semiconductor CB occurs through the Herzberg–Teller coupling term h_{C-L}, with transition moment μ_{H-C};

(2) VB to LUMO: electrons transition from the semiconductor VB to the molecular LUMO *via* μ_{V-L}, enabled by HT coupling h_{V-H}.

(3) HOMO to CB: another molecule-to-semiconductor pathway where μ_{H-B} is coupled through h_{V-H};

(4) VB to LUMO: a semiconductor-to-molecule pathway involving μ_{V-L} and HT through h_{C-L}.

In the first two pathways (1) and (2), the electrons eventually return to the HOMO (yellow arrows in Fig. 3), releasing a Raman photon and providing vibrational information on the adsorbed molecule. In the case of (3) and (4) processes, the electron transfer occurs from the HOMO to the CB or from the VB to the LUMO, followed by relaxation to the VB (grey arrows in Fig. 3b).

Strategies to enhance CM in semiconductors include introducing surface defects *via* doping or nonstoichiometric synthesis to facilitate CT pathways. For instance, transition-metal-doped TiO_2 and ZnO nanoparticles exhibit higher enhancement due to tailored defect levels that mediate CT transitions. Similarly, nonstoichiometric $W_{18}O_{49}$ nanowires with abundant oxygen vacancies promote CT with analytes like rhodamine 6G (R6G, a SERS probe molecule) through

strengthened vibronic coupling.[45] Another promising strategy is the use of amorphous semiconductor nanostructures, which possess a higher electronic density of states and localized surface states, enhancing CT efficiency. Amorphous ZnO and TiO_2 nanosheets have shown superior SERS performance due to relaxed electronic constraints and strong adsorbate coupling.[83–86]

Graphene-based substrates, although lacking a bandgap, provide a flat, delocalized π-system that enables strong orbital hybridization with adsorbed molecules and supports both ground- and excited-state CT mechanisms.[87,88] Experimental and DFT studies confirm that graphene's chemical enhancement arises from π–π interactions and symmetry-dependent charge redistribution, making it an ideal platform to probe CM effects with high precision.[75,89,90]

Recently, pyroelectric semiconductors such as $BaTiO_3$ and $BiFeO_3$, combined with graphemic materials and plasmonic materials, have been reported as excellent SERS platforms. These composites significantly contribute to the CT process, which promotes a remarkable SERS enhancement reaching approximately 5.6 to 70-fold signal amplification of common SERS probes such as R6G and MB.[91,92] Another advantage of using these semiconductor materials lies in their catalytic properties, which improves the use of the SERS technique.

Together, these insights demonstrate that chemical enhancement in SERS originates from the modulation of the molecular polarizability through CT interactions with substrate electronic states. Whether involving metal Fermi levels or semiconductor band edges, the fundamental mechanism remains rooted in orbital coupling and vibronic interactions and can be precisely tuned *via* material design and theoretical modeling. This understanding is essential for the rational design of advanced SERS substrates tailored for pesticide detection, enabling selective enhancement based on analyte–substrate interactions.[45,51,62,93,94] The practical implications of these mechanisms will be further illustrated in the following section through representative studies on SERS-based pesticide sensing.

3. SERS substrates for pesticide analysis

As already mentioned, the SERS effect relies on plasmonic resonance, so researchers have used AgNPs, AuNPs, and copper nanoparticles of various shapes and sizes to construct SERS sensors for pesticide analysis. The choice between AgNPs and AuNPs is driven by their chemical stability and plasmon resonance properties suitable for Raman spectroscopy excitation wavelengths. Typically, substrates are tailored for specific laser wavelengths to optimize enhancement.[22] Tian *et al.* (2014) explored the SERS signal for R6G employing various AuNP shapes, revealing an enhancement hierarchy: nanospheres < nanosphere aggregates < nanotriangles < nanostars. This underscores the importance of controlling the local field hotspots for optimal SERS efficiency. Additionally, the study highlighted that a 532 nm laser produced negligible SERS signals, while a 785 nm laser significantly enhanced the signal.[95]

Based on published papers, AgNPs perform better with a 532–785 nm laser, whereas AuNPs are more effective at 614–1084 nm. Another important topic is that a smaller laser wavelength may increase the fluorescence, contributing to the background signal and interference in the analysis, a challenge addressed later in this study.[96]

Effective analyte–substrate contact is essential for successful SERS measurements.[22] Many pesticides, such as Thiram, contain sulfur groups that strongly bind to metal surfaces, facilitating direct detection. This direct binding leads to characteristic Raman fingerprints that help in selective identification.[97] While direct detection is simpler for such analytes, it is less straightforward for pesticides lacking strong affinity groups, which may require surface functionalization to improve selectivity and sensitivity.

Dowgiallo and Guenther (2019) demonstrated the broad applicability of SERS using pre-aggregated ∼45 nm colloidal AuNPs to detect 21 pesticides, including fungicides and insecticides such as neonicotinoids and organothiophosphates. They reported LoDs ranging from 0.001 to 10 ppm and successfully performed simultaneous detection of phosmet and thiram in mixtures and on apple skin using principal component analysis. While the approach showcases the potential of label-free SERS for food safety applications, the absence of surface functionalization may limit sensitivity for analytes with weaker affinity to gold surfaces, particularly in more complex sample matrices.[98] Furthermore, Wei *et al.* (2025) developed an annealed Ag film substrate for thiram detection, achieving an LoD of 1.0 nmol L^{-1}. The simplicity and stability of this substrate are advantageous for practical deployment. However, the LoD, while respectable, is moderate compared to more complex nanostructures.[99]

In this sense, various strategies have been employed to produce universal SERS sensors for pesticide detection, such as a simple incubation time between nanoparticles and the target molecule before preparing the substrate.[100] Alternatively, researchers have submerged the final substrate in a contaminant solution,[101] allowed the target compound to dry on the surface,[102] or swabbed the substrate into the sample.[103] Furthermore, surface functionalization of plasmonic materials can enhance direct interactions with the analyte, thereby improving sensor selectivity.[104–106] This review brings together many papers that describe the use of SERS substrates to detect and quantify pesticides in diverse samples.

3.1 Representative studies on SERS pesticide detection

3.1.1. Plasmonic materials. Numerous studies have demonstrated the feasibility of SERS for trace-level detection of pesticides across various sample matrices. This section highlights representative studies that showcase the diversity of SERS substrate designs, detection strategies, and analytical performances, illustrating how substrate composition, sample pretreatment, and target–analyte interactions directly impact detection limits and real-world applicability.

Satani *et al.* (2023) developed a simple swab-based SERS sensor composed of cotton and fabric substrates decorated with

gold nanostars for the detection of thiram residues on fruits and vegetables. The reported LoDs ranged from 500 nmol L^{-1} to 100 μmol L^{-1}, which, while relatively high compared to other approaches, reflect the simplicity and practicality of the substrate design. Notably, the authors demonstrated the long-term stability of the sensor by monitoring the SERS signal of methylene blue over 15 weeks, during which no significant signal degradation was observed, indicating its potential for extended shelf-life and field deployment.[107]

Jiang *et al.* (2019) employed a core–shell AuNP@SiO$_2$ substrate to detect phosmet, thiabendazole, and thiram in apple samples, reporting LoDs of 0.1 mg kg^{-1}, 0.5 mg kg^{-1}, and 1.0 mg kg^{-1}, respectively. These values fall below the maximum residue limits (MRLs) established in regulatory guidelines, suggesting adequate sensitivity for food safety applications. A key distinction in this work was the use of the QuEChERS method for sample pretreatment, which significantly reduced matrix interferences and improved analyte recovery, as shown in Fig. 4. The pretreated samples were analyzed using a portable Raman spectrometer, highlighting the feasibility of *in situ* SERS-based pesticide screening in complex food matrices.[108]

Yu *et al.* (2023) reported the fabrication of a flexible, eco-friendly SERS substrate based on cellulose diacetate (CDA) integrated with AuNPs. This biosourced platform achieved an LoD of 0.1 μmol L^{-1} for thiram in residual water, demonstrating a balance between analytical performance, environmental sustainability, and production scalability.[109] In another approach, Xie *et al.* (2022) transferred AuNPs onto a poly-dimethylsiloxane (PDMS) membrane to detect thiram on fruit peels, obtaining a notably lower LoD of 9.3 nmol L^{-1}. Recovery values from real samples ranged from 98.7% to 104.9%, underscoring the accuracy and reliability of the substrate.[110]

Taken together, these studies illustrate the wide variation in analytical performance for thiram detection based on differences in substrate composition, architecture, and analytical context. The cotton-based substrate[107] prioritized simplicity and durability over sensitivity, whereas the PDMS-based design[110] leveraged enhanced hotspot generation to achieve superior detection limits. The CDA-based platform[109] represented an environmentally conscious compromise, with moderate LoD values and scalable fabrication. Meanwhile, Jiang *et al.* (2019) demonstrated the value of integrating effective sample pretreatment with nanostructured substrates to overcome matrix complexity and enable multi-residue detection within regulatory limits.[108] It is important to highlight that the lowest LoD is not the only focus when developing a SERS substrate; reusability, reproducibility, large-scale production, and many other factors are also involved. In summary, the best substrate is the one that fits the specific application demand.

Besides the use of thiram, some studies have explored the SERS detection of pesticides from other chemical classes. Ly *et al.* (2019) studied the correlation between SERS and DFT of fipronil, a phenylpyrazole pesticide, adsorbed on AgNPs. Because fipronil has low solubility in aqueous media, the authors used a surfactant (cetyltrimethylammonium chloride) in the prepared substrate, obtaining a LoD of 2.29 nmol L^{-1} [111]. By combining SERS with DFT calculations, the authors identified selective enhancement through the nitrile group, demonstrating the method's potential for sensitive and cost-effective pesticide monitoring.

It is possible to highlight the study of Chen *et al.* (2019), who developed a stable substrate comprising nanocellulose (NC) decorated with AgNPs with a stability of 60 days. This jelly-like material was used as a substrate to quantify thiabendazole, a benzimidazole fungicide, in apple and cabbage peels, as depicted in Fig. 5. Using a portable self-developed Raman spectrometer equipped with a 785 nm laser at 120 mW power, the system demonstrated impressive efficiency with a LoD of 10 nmol L^{-1} for R6G and 5.0 ng cm^{-2} for thiabendazole. This study illustrates the capability and innovation of SERS analysis in addressing modern analytical challenges.[112] Another study exploring benzimidazole detection was conducted by Oliveira
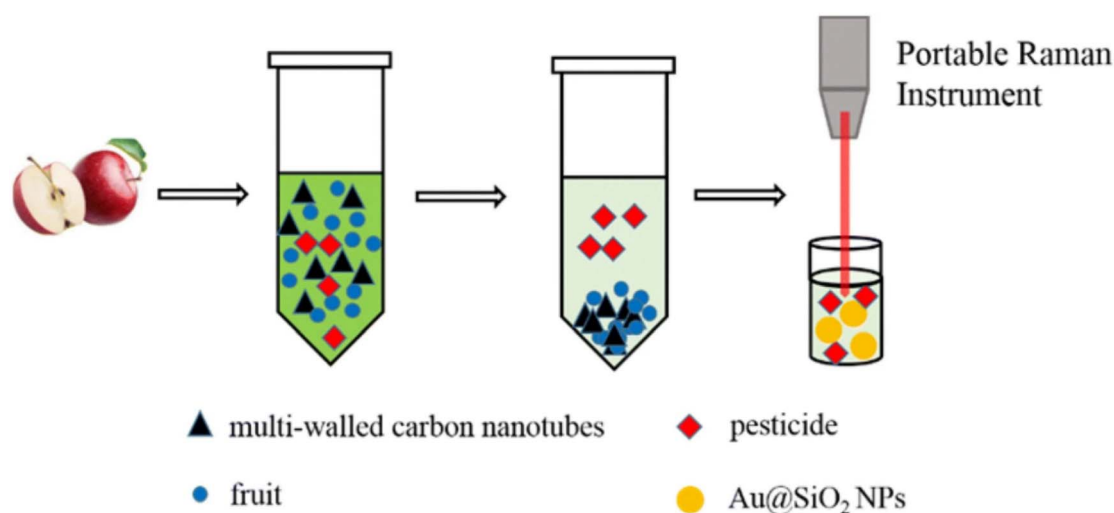

Fig. 4 Scheme of the sample pretreatment with multi-walled carbon nanotubes, for the clean-up of the matrix, and detection with SERS using a portable Raman instrument. This figure has been adapted/reproduced from ref. 108 with permission from Springer Nature, copyright 2025.
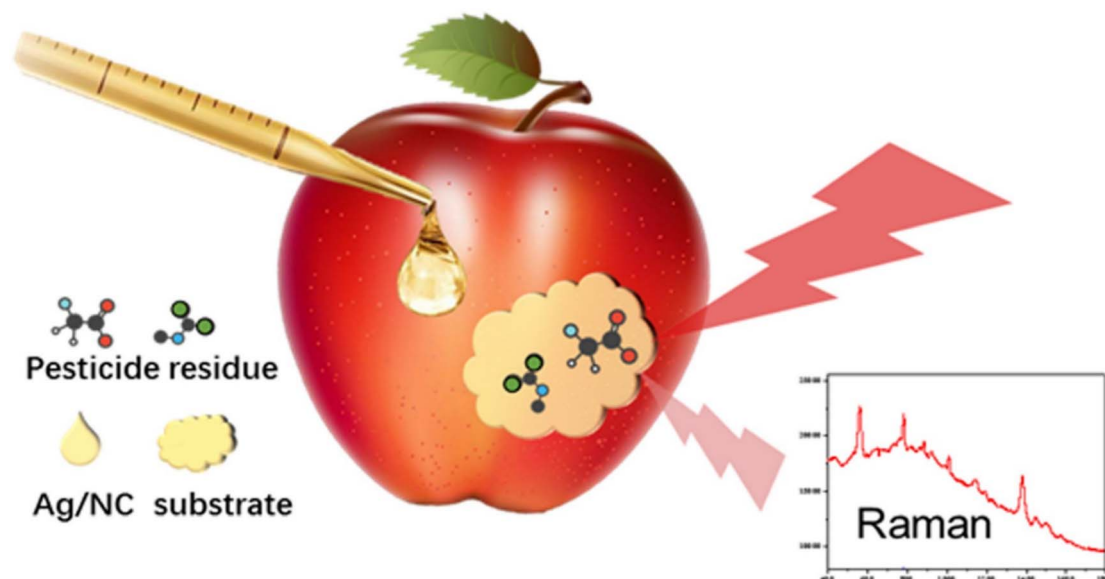
Fig. 5 Scheme for SERS analysis of thiram and thiabendazole in apple peels using AgNP@NC as the substrate. This figure has been adapted/reproduced from ref. 112 with permission from Elsevier, copyright 2025.

et al. (2024), which investigated the SERS detection of thiabendazole, a benzimidazole fungicide, using colloidal AgNPs aggregated with NaCl. They achieved a LoD of 0.1 μmol L^{-1} and demonstrated that controlled aggregation significantly influenced signal intensity by modulating hotspot density. Importantly, their findings suggested that π–metal interactions between the benzimidazole ring and the gold surface can facilitate strong adsorption even in the absence of sulfur or thiol groups. The method provided a linear response over a broad concentration range, highlighting its potential for trace analysis.[113]

Chen *et al.* (2024) demonstrated the label-free SERS detection of six triazole pesticides using gold decahedral nanoparticles, achieving remarkable sensitivity and the ability to perform *in situ* measurements on the surfaces of fruits and vegetables. The reported LoDs for each analyte were notably low: triadimefon, approximately 2.84 nmol L^{-1}; triazophos, 0.47 nmol L^{-1}; myclobutanil, 0.76 nmol L^{-1}; difenoconazole, 0.50 nmol L^{-1}; epoxiconazole, 0.58 nmol L^{-1}; and diniconazole, 0.55 nmol L^{-1}. These values highlight the exceptional detection capabilities of the system in the sub-nanomolar range. The use of the nanostructured substrate allowed the acquisition of distinct Raman fingerprints for each pesticide, which, when analyzed with a multivariate approach such as principal component analysis (PCA), enabled reliable identification and quantification of multiple triazole residues simultaneously.[114]

Among the various pesticides analyzed by SERS, glyphosate stands out due to its widespread agricultural use and analytical complexity, serving as a benchmark for evaluating SERS performance.[115] A significant contribution to this understanding was made by Mikac *et al.* (2022), who systematically compared AgNPs and AuNPs combined with different excitation wavelengths (532, 632, and 785 nm), as shown in Fig. 6. Their results showed that AgNPs at 532 nm yielded the highest SERS

intensities for glyphosate, with a detection limit of 1.0 mmol L^{-1}, while AuNPs at 785 nm achieved a lower LoD of 100 μmol L^{-1}. Functionalizing AuNPs with cysteamine further improved detection to 10 μmol L^{-1}, due to enhanced electrostatic interactions between the amine-modified surface and the analyte.[106]

More importantly, these findings reinforce the critical importance of matching the nanoparticle LSPR with laser excitation and tailoring the nanoparticle surface chemistry to favor analyte adsorption. For instance, Murcia-Correa *et al.* (2023) fabricated low-cost substrates using DVD-R polycarbonate disks coated with thin layers of silver. This approach enabled detection of glyphosate down to 100 nmol L^{-1} for pure glyphosate and 1.0 μmol L^{-1} in Roundup™ commercial formulations, demonstrating how nanostructured surface morphology and reproducibility directly affect analytical sensitivity.[116] Emonds-Alt *et al.* (2022) demonstrated a microfluidic SERS platform using *in situ* synthesized silver nanoparticles for rapid glyphosate detection in various water samples. By adding borax buffer (pH 9) and sodium nitrate, they optimized conditions to enhance glyphosate adsorption. Using a 647 nm laser in a flow cell setup, they achieved a detection limit of 237 nmol L^{-1}, highlighting the potential of integrating microfluidics and SERS for sensitive, real-time environmental monitoring.[117]

One limitation of plasmonic substrates lies in their inherent susceptibility to degradation over time. Factors such as oxidation, surface fouling, and damage from intense laser excitation can lead to a gradual decline in signal enhancement and overall performance. Additionally, many plasmonic substrates are designed as single-use consumables, lacking the durability and reusability desirable for cost-effective and sustainable applications. These challenges have motivated the exploration of alternative materials and hybrid systems, particularly semiconductor-based substrates, which offer enhanced stability, photocatalytic properties, and the potential for self-
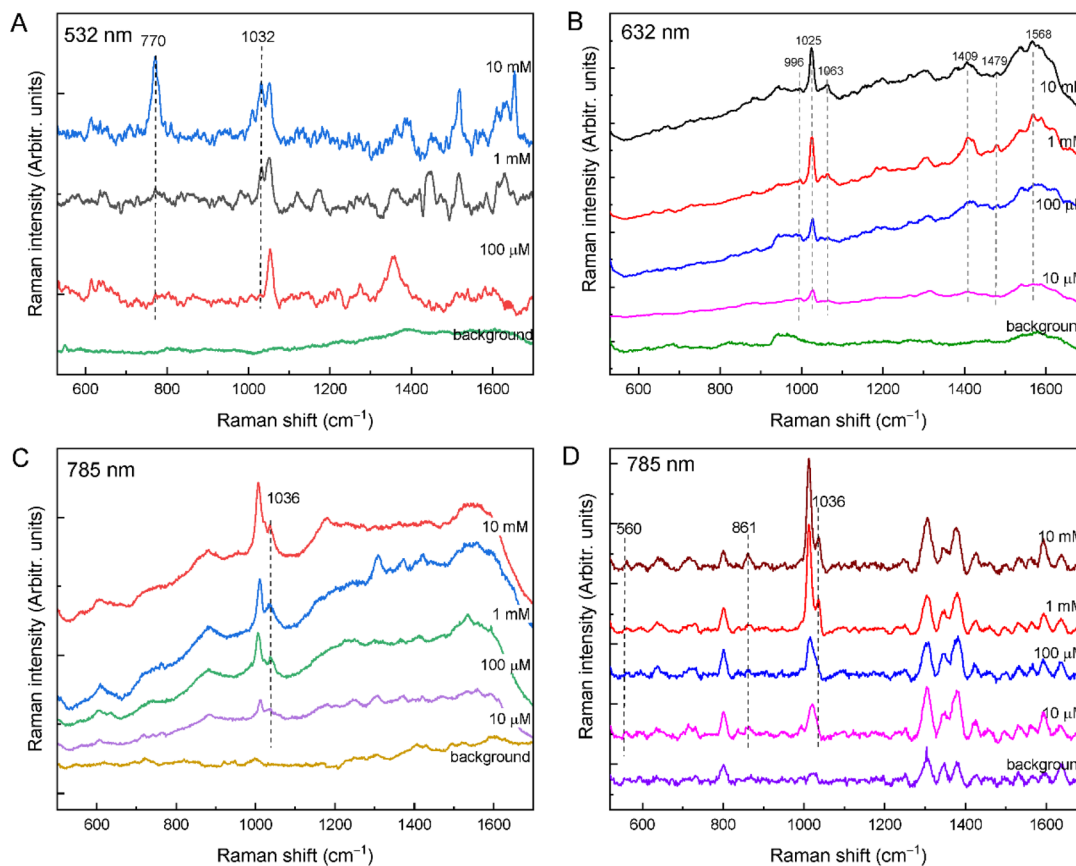
Fig. 6 SERS spectra of different glyphosate concentrations: (A) with Ag NPs at 532 nm excitation; (B) with Au NPs at 632 nm excitation; (C) with Au NPs at 785 nm excitation; (D) with Au NPs at 785 nm excitation (baseline corrected; portable Raman). This figure has been adapted/reproduced from ref. 106 with permission from MDPI, copyright 2025.

cleaning and regeneration, thereby addressing some of the key drawbacks of purely plasmonic platforms.[118]

3.1.2. Use of semiconductor materials combined with a plasmonic SERS substrate. In response to the limitations of plasmonic materials, semiconductor-based substrates have emerged as a promising class of SERS platforms. These materials not only offer improved chemical stability and resistance to photothermal damage, but also open avenues for exploiting charge transfer mechanisms underlying CM. By tailoring band structures, surface states, and defect engineering, semiconductors enable alternative enhancement routes beyond purely electromagnetic effects, broadening the scope of SERS applications in analytical chemistry.

For this, Jin *et al.* (2025) introduced a recyclable paper-based SERS substrate integrating AgNPs and ZnO nanoparticles (ZnONPs), which enabled sensitive detection and photocatalytic degradation of deltamethrin and atrazine. With LoDs of around 87.1 nmol L^{-1} for deltamethrin and 183.2 nmol L^{-1} for atrazine, the platform met environmental standards for agricultural water. The ZnO semiconductor component played a dual role: enhancing charge-transfer-mediated SERS sensitivity and enabling photocatalytic self-cleaning under UV light.[119] Notably, the system retained its detection capacity after multiple uses, while theoretical studies using DFT clarified the hydrolysis

mechanisms and degradation sequence, showing that atrazine degrades before deltamethrin. This work highlights the potential of semiconductor-assisted SERS substrates not only for detection but also for mechanistic investigation and environmental remediation.[119]

Tu *et al.* (2025) developed a dual-ligand Cu-based MOF nanoprobe with remarkably low background fluorescence for fast screening and sensitive detection of glyphosate. The probe operates *via* ligand-to-metal charge transfer (LMCT) and photoinduced electron transfer (PET). It exhibited a linear response from 0.1 to 80 μmol L^{-1} and a detection limit of 33 nmol L^{-1}, well below the 4.1 μmol L^{-1} safety threshold set by the U.S. Environmental Protection Agency, demonstrating strong analytical performance for environmental monitoring.[120]

Ye *et al.* (2022) synthesized a dual-MOF material by modifying ZnO@Co$_3$O$_4$ with AgNPs. This novel material forms a heterojunction that enhances charge transfer, resulting in a 6.6-fold signal increase compared with the ZnO@AgNP material. The porous nature of this material, combined with plasmonic AgNP, allows for achieving LoDs of 1.0 nmol L^{-1}, 10.0 nmol L^{-1}, and 100 nmol L^{-1} for triazophos, fonofos, and thiram, respectively. The authors demonstrated excellent reproducibility of the substrate (RSD = 8.0%) and successfully applied it to the analysis of tea and dendrobium leaves.[121]

Lai *et al.* (2022) analyzed thiram, diquat, and paraquat using core–shell AuNP@AgNP decorated on a 2D nickel metal–organic framework (Ni-MOF) substrate, obtaining LoDs of 362, 549, and 34.6 nmol L^{-1}, respectively. The presence of Ni-MOF enhances the CM, increasing the charge transfer from the substrate to the analyte through the HOMO–VB–LUMO pathway when exposed to laser excitation during SERS analysis. The authors reported that the substrate exhibited excellent stability (5 weeks) and good reproducibility, with a relative standard deviation (RSD) of 8.8% ($n = 25$).[122] Wang *et al.* (2023) developed a reusable substrate based on silver nanoflowers (AgNFs) on zinc oxide nanorods (ZnO NRs). According to the authors, the synergic effect of AgNF@ZnO NRs enhances the EM and charge transfer effect, leading to a LoD of 0.1 pmol L^{-1} for crystal violet (SERS probe molecule). Moreover, the degradation rate reached 98.59% after 30 min of irradiation, with no detectable SERS signal, and this performance was maintained for at least four consecutive cycles. The strategy used by the authors to quantify the pesticide thiram in apple peel and river water was to deposit the AgNF@ZnO NRs on the surface of adhesive tape, as shown in Fig. 7. This approach achieved detection at a concentration of 1.0 μmol L^{-1} in river water. The renewability of the SERS substrate surface depends on the photocatalytic properties of ZnO. Therefore, analytes can undergo degradation under light irradiation.[123]

Ji *et al.* (2019) developed a substrate in a two-step synthesis by depositing a Cu_2O nanoarray on the surface of indium tin oxide (ITO) glass, followed by the reduction of $AgNO_3$ on the substrate surface. Thus, the authors claimed that the surface became reusable because this material has photocatalytic properties and can degrade the analyte adsorbed on the surface. In addition to not employing the substrate to analyze pesticides, the author showed that the proposed SERS substrate was able to quantify R6G at 1.0 pmol L^{-1}.[124]

These discussions highlight the critical role of plasmonic and semiconductor materials in enabling sensitive and effective SERS-based detection. Their unique optical and electronic properties contribute significantly to signal enhancement and substrate performance. Table 1 summarizes additional studies that employed these materials for the quantitative detection of pesticides, illustrating the diversity of substrate designs and analytical strategies in the field.

3.1.3. Graphenic materials. Graphene materials are considered zero-bandgap semiconductors and have emerged as an alternative since they are particularly advantageous because of their unique properties, such as high surface area and strong adsorption capabilities. In graphene, the remaining $2p_z$ orbital of each sp^2-hybridized carbon atom forms an extensive delocalized π–bond network, which significantly enhances the chemical interactions with the target molecule.[143–146] Recent
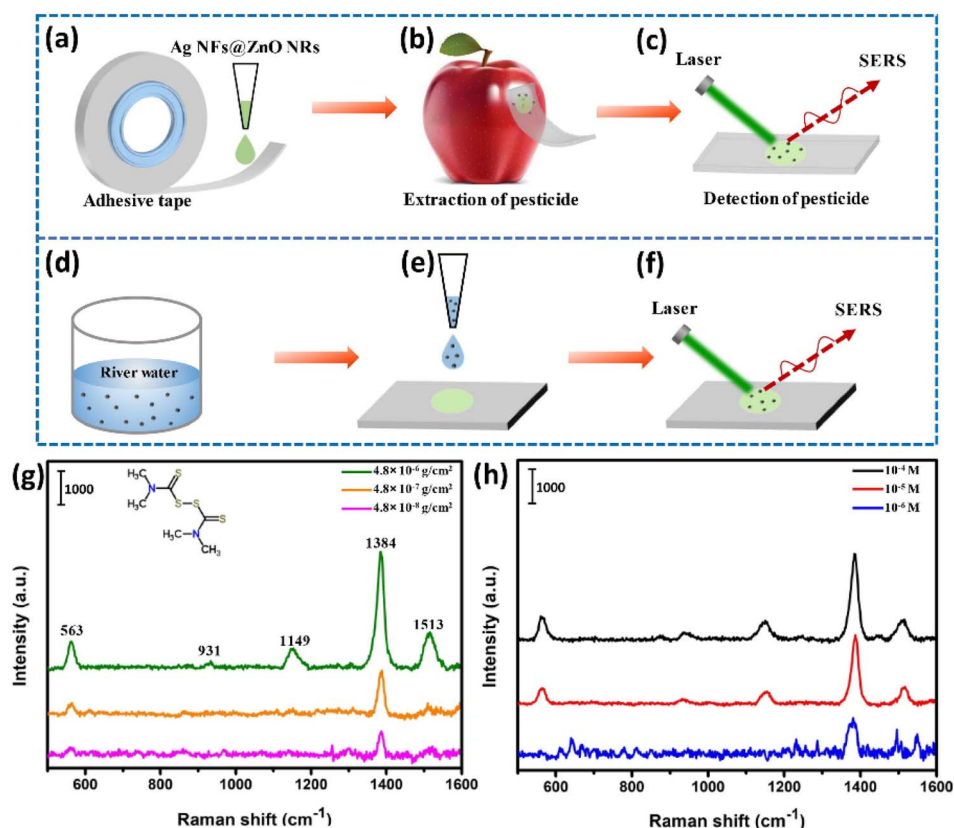
Fig. 7 Scheme illustrating (a)–(c) the procedure of preparing a flexible SERS substrate for extracting and detecting pesticides on apple surfaces. (d)–(f) Schematic showing the SERS detection of pesticides in river water. (g) SERS spectra of thiram with different concentrations extracted from the apple surface. (h) SERS spectra of thiram in river water. This figure has been adapted/reproduced from ref. 123 with permission from Springer Nature, copyright 2025.

Table 1 Comparative table of SERS substrates utilizing plasmonic and semiconductor materials for pesticide quantification

Plasmonic and semiconductor materials				
Pesticide	Samples	Substrate	Limit of detection	References
Fipronil	—	AgNP	2.29 nmol L^{-1}	111
Phosmet	Apple	Au@SiO$_2$NP	0.5 mg kg^{-1}	108
Paraquat	Fruit peel	AgNP colloidal	1.0 nmol L^{-1}	125
Tricyclazone	Rice	AgNP colloidal	0.002 mg L^{-1}	126
Glyphosate	—	AgNPs	1.0 mmol L^{-1}	106
Glyphosate	—	AuNPs	100 μmol L^{-1}	106
Parathion-methyl	Fruit peel	Tape-AuNPs	2.6 ng cm^{-2}	127
Thiram	Fruit peel	Tape-AuNPs	0.24 ng cm^{-2}	127
Chlorpyrifos	Fruit peel	Tape-AuNPs	3.51 ng cm^{-2}	127
Glyphosate	Drinking water-	AgNPs	40.0 μg L^{-1}	117
Triadimefon	Fruits and vegetables	Au decahedral	2.84 nmol L^{-1}	114
Triazophos	Fruits and vegetables	Au decahedral	0.47 nmol L^{-1}	114
Myclobutanil	Fruits and vegetables	Au decahedral	0.76 nmol L^{-1}	114
Difenoconazole	Fruit and vegetables	Au decahedral	0.50 nmol L^{-1}	114
Epoxiconazole	Fruits and vegetables	Au decahedral	0.58 nmol L^{-1}	114
Diniconazole	Fruits and vegetables	Au decahedral	0.55 nmol L^{-1}	114
Thiram	Fish scale and leaf surface	AgNP@AgNW	0.1 nmol L^{-1}	65
Malachite green	Fish scale and leaf surface	AgNP@AgNW	0.01 nmol L^{-1}	65
Methomyl	Tea	AgNPs	0.558 ng L^{-1}	128
Acetamiprid	Tea	AgNPs	0.188 ng L^{-1}	128
2,4-D	Tea	AgNPs	4.72 ng L^{-1}	128
Thiram	Fruits	3D-Au@PDMS	9.3 nmol L^{-1}	110
12 pesticides	—	AuNPs	10 ppm	129
Thiram	Tea and dendrobium leaves	ZnO@Co$_3$O$_4$@AgNPs	0.1 μmol L^{-1}	121
Fonofos	Tea and dendrobium leaves	ZnO@Co$_3$O$_4$@AgNPs	10 nmol L^{-1}	121
Triazophos	Tea and dendrobium leaves	ZnO@Co$_3$O$_4$@AgNPs	1.0 nmol L^{-1}	121
Thiram	Fruits and vegetables	AgNP/nanocellulose substrate	0.5 ng cm^{-2}	112
Thiabendazole	Fruits and vegetables	AgNP/nanocellulose substrate	5 ng cm^{-2}	112
Chlorpyrifos	Apple	AgNP/glass bead	10 ng mL^{-1}	100
Thiabendazole	—	AgNP	0.1 μmol L^{-1}	113
Imidacloprid	Apple	AgNP/glass bead	50 ng mL^{-1}	100
Chlorpyrifos	Tea	AgNP flowerlike	0.1 nmol L^{-1}	102
Thiram	Water	AuNP@CDA	0.1 μg L^{-1}	109
Green malachite	—	PVA nanofiber@Au	10.0 nmol L^{-1}	130
Crystal violet	Apple peel and river water	AgNF@ZnO NR	0.1 pmol L^{-1}	123
Acephate	Pear peel	AuNF/CW-35	1.0 pg mL^{-1}	131
Hexachlorobenzene	Soil	Ag Fe-NP 3D	1.0 mmol L^{-1}	132
Thiram	—	Au@Ag nanoplate-in-shell	12.29 nmol L^{-1}	133
Chlorothalonil	—	Au@Ag nanoplate-in-shell	30.15 nmol L^{-1}	133
Thiram	Fruits and vegetables	2D Ni-MOF-Au@AgNP	362 nmol L^{-1}	122
Diquat	Fruits and vegetables	2D Ni-MOF-Au@AgNP	549 nmol L^{-1}	122
Paraquat	Fruits and vegetables	2D Ni-MOF-Au@AgNP	34.6 nmol L^{-1}	122
Glyphosate	Roundup™	DVD-R@AgNP	0.1 μmol L^{-1}	116
Thiram	—	Annealed Ag	1.0 nmol L^{-1}	99
Lindane	—	AgNPs	0.1 nmol L^{-1}	134
Deltamethrin	Ground water	Paper-based AgNP@ZnONPs	87.1 nmol L^{-1}	119
Atrazine	Ground water	Paper-based AgNP@ZnONPs	183.2 nmol L^{-1}	119
Thiram	Apple juice	Au@Ag	76 nmol L^{-1}	135
Acetamiprid	Apple juice	Au@Ag	1.22 μmol L^{-1}	135
Fenthion	Cowpeas and peppers	Fe$_3$O$_4$–COOH@UiO-66/Au@Ag	12.1 pg kg^{-1}	136
Triazophos	Cowpeas and peppers	Fe$_3$O$_4$–COOH@UiO-66/Au@Ag	2.96 μg kg^{-1}	136
Thiram	Water sample	CC/ZnO–Ag@ZIF-8	1.0 nmol L^{-1}	137
Thiram	Apple	CNF-AgNPs	58.1 nmol L^{-1}	138
Thiabendazole	Apple	CNF-AgNPs	96.3 nmol L^{-1}	138
Thiram	Fish and apple	Fe$_3$O$_4$@Au@Ag@Au	0.18 ng cm^{-2}	139
Methyl parathion	Apple peel	Au-core/Ag-shell nanocubes and AuNSs	0.38 nmol L^{-1}	140
Thiram	—	AuNPs	0.42 μmol L^{-1}	141
Thiabendazole	—	AuNPs	4.96 μmol L^{-1}	141
Thiram	Apple surface	Cellulose nanofiber – AgNPs	0.047 ng cm^{-2}	142

studies have demonstrated the fabrication of graphene-based hybrids as SERS substrates.[147,148] Graphene and its derivatives—such as graphene oxide (GO) and reduced graphene oxide (rGO)—are two-dimensional (2D) carbon nanosheets. Graphene-based hybrids are attractive as SERS substrates not only because the metal nanoparticles deposited on graphene could enhance the SERS intensity *via* the EM mechanism and facilitate the charge transfer between graphene and adsorbed molecules, contributing to the CM mechanism, but also because the 2-D planar structure of graphene provides a flat surface for the uniform deposition of metal nanoparticles which is helpful for the improvement in the uniformity of the SERS signal.[149]

Besides, incorporating graphene with semiconductor metals such as TiO_2 and ZnO into plasmonic materials makes the degradation of pollutants feasible.[101,121,123,150,151] This allows the reuse of substrates and enhances their durability and sustainability. As described by Liu *et al.* (2022), one of the significant obstacles to utilizing SERS substrates is their limited reusability.[29]

Using a recyclable substrate addresses several challenges in SERS analysis, particularly by enhancing the accessibility for mass production and rendering it a viable option for research laboratories involved in large-scale analyses. However, another problem is that fluorescence can significantly interfere with the Raman signal. Based on this feature, Xie *et al.* (2009) observed the ability of graphene to promote the quenching of R6G fluorescence.[152] Consequently, the use of graphene can be highlighted for its several beneficial properties in manufacturing SERS substrates, which will then be discussed.[153,154]

Sun *et al.* (2017) described an effective strategy for improving the reusability of substrates by incorporating graphene into their composition. Their substrate, composed of polymethyl methacrylate (PMMA), AgNPs, and graphene, was used to quantify thiram, achieving a good LoD of 1.0 μmol L^{-1}. To assess the reusability of the substrate, the thiram-contaminated material was immersed in an ethanol solution for four hours to dissolve the pesticide, allowing its subsequent reuse. After cleaning, the PMMA/AgNP/graphene substrate showed no residual signals, confirming the method's effectiveness. The researchers successfully reused the substrate thrice, demonstrating remarkable signal repeatability. Thus, the exposed graphene not only prevents contamination of samples and makes SERS analysis environmentally friendly and non-invasive but also shows efficient reusability through a rapid adsorption–desorption process of pesticides in water.[155] Another critical aspect to highlight is the work by Atta, Sharaf, and Vo-Dinh (2024), who developed a solution-based SERS platform using graphene oxide-coated silver–gold nanostars (GO-SGNS) to enable highly sensitive and reproducible detection of multiple pesticides in water and directly on apple surfaces.[156] Integrating graphene oxide into the plasmonic nanostar architecture improved colloidal stability and enhanced SERS signals through the combined effects of electromagnetic hotspots and charge-transfer interactions. The platform achieved detection limits as low as 10 pmol L^{-1} for ziram, 50 pmol L^{-1} for phorate, and 100 pmol L^{-1} for triazophos and azinphos-methyl, values below regulatory thresholds. Quantitative analysis followed a one-site binding model, with AEFs reaching up to 3.2×10^8.[156] These findings underscore the strong analytical capability of
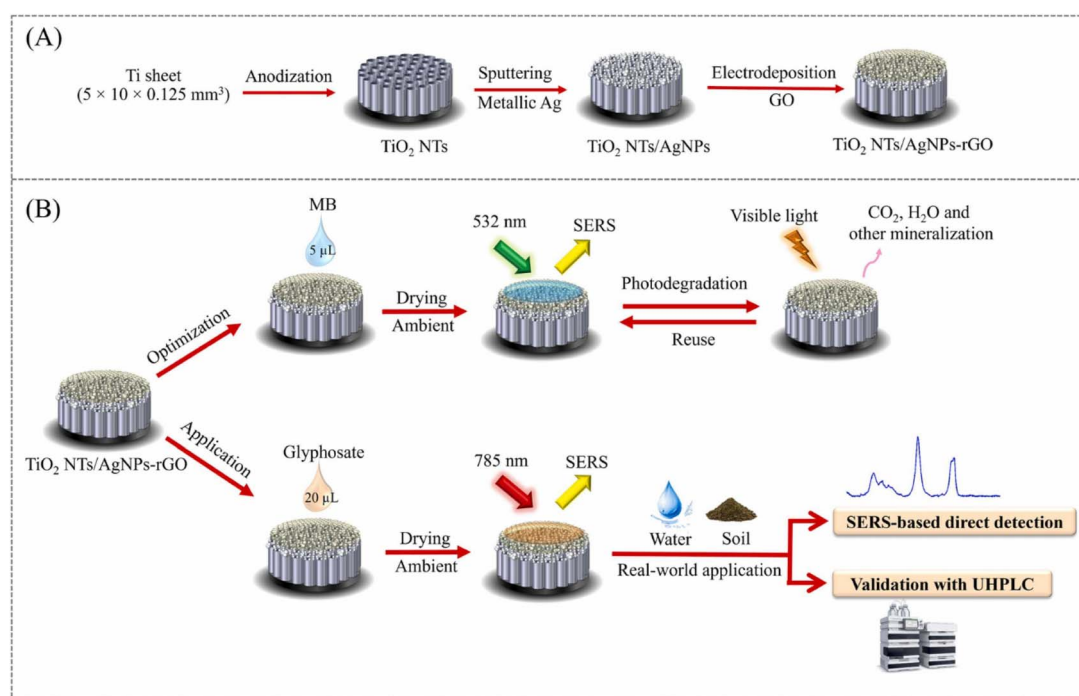

Fig. 8 Scheme of (A) fabrication of the TiO_2 NTs/AgNPs–rGO SERS substrate and (B) optimization and real application of the SERS substrate. This figure has been adapted/reproduced from ref. 151 with permission from Elsevier, copyright 2025.

GO-SGNS for rapid, ultra-trace pesticide detection and reinforce the value of graphenic–plasmonic hybrids in solution-based SERS sensing.

Moreover, rGO can amplify SERS signals because of its excellent adsorption capacity. It provides additional CM enhancement by facilitating charge transfer between the extensive π–π conjugated structure of rGO and the target molecules. Butmee, Samphao, and Tumcharern (2022) developed a sensor employing a vertical heterostructure of rGO over a double-layer of AgNPs on titania nanotubes (TiO$_2$ NTs), as illustrated in Fig. 8. The authors described the excellent performance of the TiO$_2$ NTs/AgNPs-rGO substrate in quantifying glyphosate, achieving a LoD of 17.7 nmol L^{-1}. Furthermore, photocatalytic regeneration tests demonstrated complete degradation of MB after each irradiation cycle, with the regenerated substrate retaining 96.4% of its initial SERS intensity after three reuse cycles before a marked decline in the fourth cycle, attributable to silver nanoparticle rearrangement and aggregation. In addition, the TiO$_2$ NTs/AgNPs-rGO substrate exhibited excellent shelf-life stability, showing less than 6% signal variation after 30 days of storage, and maintained over 91.9% of its initial SERS intensity after 180 days under ambient conditions. This work highlights the powerful synergy between graphene-based materials, semiconductor metal oxides, and plasmonic nanoparticles in enhancing both EM and CM of SERS, enabling one of the lowest detection limits reported among plasmonic and semiconductor-based substrates in this review. Moreover, the substrate was reusable because the presence of rGO and TiO$_2$ NTs enhanced the photodegradation of the analyte on the surface.[151]

GO has been shown to enhance the adsorption of pesticides through π–π stacking and electrostatic interactions. This was explored and demonstrated by Ma *et al.* (2018), who utilized AgNPs and GO to formulate ink for screen-printed SERS paper

substrates, as illustrated in Fig. 9. Employing this innovative disposable sensor, the researchers were able to effectively monitor thiram, thiabendazole, and methyl parathion, achieving limits of detection (LoD) of 0.26 ng cm^{-2}, 28 ng cm^{-2}, and 7.4 ng cm^{-2}, respectively. To detect pesticides, the researchers employed the sensor as a swab on the surfaces of fruits and vegetables, successfully quantifying the three pesticides simultaneously, with recovery values ranging between 96% and 98%.[103] Moreover, Song *et al.* (2020) applied GO composites combined with Au@Ag to investigate thiram using a silanized quartz slide. First, they immersed the slide in a solution of GO, washed it, and then immersed it in a colloidal solution of Au@Ag. According to the study, the authors reported a LoD of 26.2 μmol L^{-1} for thiram. In contrast, the LoDs for apple and grape juice samples without pretreatment were 153 and 559 μmol L^{-1}, respectively.[157]

Wang *et al.* (2019) explored the use of graphene to enhance the SERS signal and synthesized Ag nanoplates on graphene sheets. The authors affirmed that Ag nanoplates held by graphene created hotspots, leading to an EM effect. Moreover, graphene sheets can serve as a CM because of their strong absorption ability and π–π interactions with pesticide molecules. Ag-nanoplate@graphene was spin-coated on a silicon wafer substrate and enabled the detection of thiram with an LoD of 40 nmol L^{-1}.[158] Daoudi *et al.* (2022) evaluated the Ag/GO/silicon nanowire (SiNW) substrate's potential for detecting atrazine. The SERS substrate was produced by spin-coating GO onto silicon nanowires and depositing AgNPs *via* drop casting. The material showed excellent performance in quantifying atrazine, achieving a picomolar-level LoD of 2.0 pmol L^{-1}. The mechanism involves electron transfer from the conduction band of the SiNW to GO, which allows electrons to flow to the AgNP conduction band. GO is a zero-bandgap semiconductor that enables free electron movement to the AgNP conduction
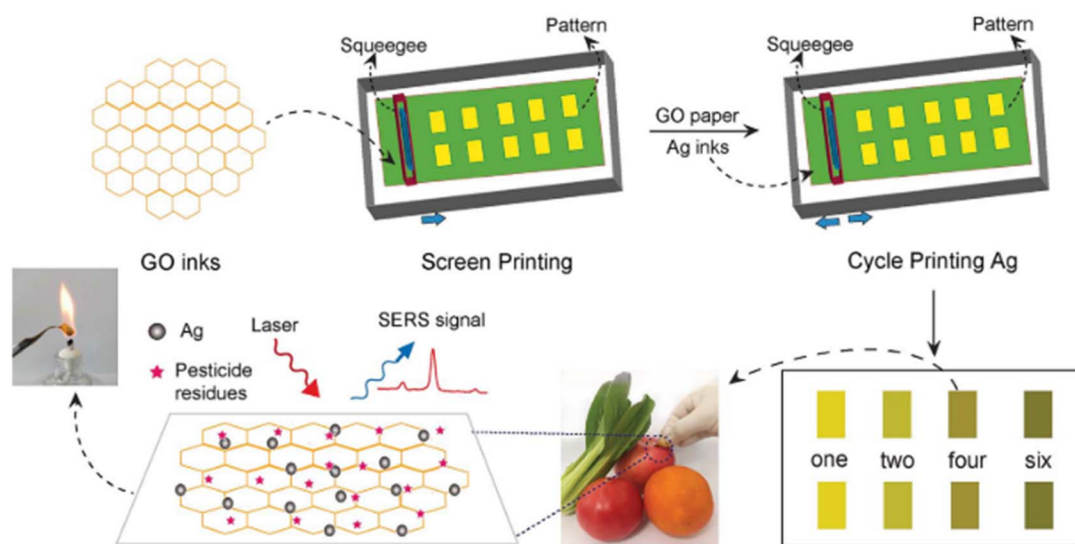

Fig. 9 Scheme illustrating the fabrication process of the SERS paper by screen-printing and its use as a swab to quantify thiram, thiabendazole, and methyl parathion in fruits and vegetables. This figure has been adapted/reproduced from ref. 103 with permission from Royal Society of Chemistry, copyright 2025.

band, followed by the flow of conduction band electrons to the atrazine HOMO. The free electrons in GO can be directly transferred to the HOMO of the analyte molecules, thereby contributing to the SERS effect.[66]

Although graphene is formally a semiconductor, its two-dimensional structure, π-conjugation, and tunable surface chemistry endow it with distinct physicochemical properties, justifying its treatment as a separate class of SERS substrates, as reflected in the studies summarized in Table 2.

3.1.4. Advantages of biorecognition in SERS. One drawback of SERS detection is selectivity because the analyte signal can be overlapped by interferents in complex matrices.[28,169] Thus, when considering new approaches for pesticide detection, many authors have described the use of biorecognition, such as antibody–antigen interactions, aptamers, and MIPs, to enhance the selectivity of the SERS method.[104,132] Biorecognition is advantageous due to its easy conjugation with plasmonic materials, high specificity for the pesticide of interest, low cost, and ease of production.

Kamkrua et al. (2023) developed a SERS-based aptasensor for detecting paraquat, a bipyridylium herbicide, by functionalizing commercial Au nanoparticle substrates (59 ± 17 nm) with

a thiol-modified aptamer. The authors achieved a LoD of 0.10 μmol L^{-1}, which was not the lowest reported for paraquat; however, the aptasensor exhibited remarkable selectivity. It effectively distinguished paraquat from structurally similar herbicides and insecticides and maintained strong performance in real water samples. These results underscore the advantage of integrating molecular recognition elements into SERS platforms for improving selectivity in complex matrices.[170]

Zhao et al. (2024) developed a portable and selective SERS platform for detecting fenthion pesticides by integrating gold nanoparticle monolayers with molecularly imprinted polymers (MIPs).[171] Using a sulfhydryl-assisted interfacial self-assembly method, AuNP monolayers were immobilized on mercapto-silicon wafers, forming stable S–Au bonds that ensured structural integrity during surfactant removal. In situ UV-induced polymerization of MIPs on the AuNP surface endowed the substrate with specific recognition capabilities for fenthion. The sensor achieved a detection limit as low as 1.0 nmol L^{-1} in standard solutions and 10 nmol L^{-1} in complex pesticide mixtures, with excellent uniformity (RSD = 3.67%) and reproducibility (RSD = 10.40%). Notably, the platform selectively detected fenthion even in the presence of structurally related

Table 2 Overview of graphenic materials applied in SERS platforms for pesticide quantification

Graphenic materials

Pesticide	Samples	Substrate	Limit of detection	References
Thiram	Apple and grape juice	Au@AgNP/GO	26.2 μmol L^{-1}	157
Azinphos-methyl	—	G/Au/AuNR	5.0 ppm	159
Carbaryl	—	G/Au/AuNR	5.0 ppm	159
Phosmet	—	G/Au/AuNR	9.0 ppm	159
Thiram	Grape juice	Au@AgNP/GO/Au@AgNP	0.1 μmol L^{-1}	160
Glyphosate	Water and soil	TiO$_2$ NT/AgNP@rGO	17.7 nmol L^{-1}	151
Thiram	Fruits and vegetables	AgNPs/GO	0.26 ng cm^{-2}	103
Thiabendazole	Fruits and vegetables	AgNPs/GO	28 ng cm^{-2}	103
Methyl parathion	Fruits and vegetables	AgNPs/GO	7.4 ng cm^{-2}	103
Thiram	—	AgNC@rGO	44.0 nmol L^{-1}	145
Ferbam	—	AgNC@rGO	38.0 nmol L^{-1}	145
Thiram	Drinking water	AgNC@GO@AuNP	0.37 ppb	161
Thiabendazole	Drinking water	AgNC@GO@AuNP	8.3 ppb	161
Thiram	Grape juice	Au@Ag NPs/GO/Au@Ag NPs	0.1 μmol L^{-1}	160
Thiram	—	AgNP@GH	40 nmol L^{-1}	158
Methyl parathion	—	AgNP@GH	600 nmol L^{-1}	158
Thiram	—	rGO-Au@AgNR	5.12 nmol L^{-1}	162
Green malachite	—	Ag$_{nanocube}$/GO	1.0 nmol L^{-1}	163
Methylene blue	—	Ag$_{nanocube}$/GO	0.1 nmol L^{-1}	163
Crystal violet	—	Ag$_{nanocube}$/GO	1.0 nmol L^{-1}	163
Tetramethylthiuram disulfide	—	Ag$_{nanocube}$/GO	10 nmol L^{-1}	163
Diquat dibromide	—	Ag$_{nanocube}$/GO	10 nmol L^{-1}	163
Thiram	Apple juice	PMMA/AgNP/Graphene	1.0 μmol L^{-1}	155
Paraquat	Fruit peel	Gr/Au/RP PMMA	10 nmol L^{-1}	164
2,4 D	Fruit peel	Gr/Au/RP PMMA	1.0 μmol L^{-1}	164
Thiram	Fruit peel	Fe$_3$O$_4$@GO@Ag	0.48 ng cm^{-2}	143
Thiabendazole	Fruit peel	Fe$_3$O$_4$@GO@Ag	40 ng cm^{-2}	143
Methyl parathion	Apple	G/AgNP/PI	68 ng cm^{-2}	146
Thiram	Orange juice	AgNP/Graphene paper	1.0 μmol L^{-1}	165
Atrazine	—	Ag$_{nanoprisme}$/GO/SiNW	2.0 pmol L^{-1}	66
Thiram	Orange peel	AuNP/G/AuNP	0.24 ppm	166
Thiabendazole	American Cherry	Layered Au/Ag/G/PDMS	10^{-8} mg mL^{-1}	167
Fenvalerate	—	Ag/rGO	16.9 ng kg^{-1}	168

pesticides in seawater, highlighting the synergy between SERS sensitivity and MIP-based molecular recognition for real-sample analysis. Wan *et al.* (2022) reported a SERS sensor for diazinon detection using Zr-based MOFs (UiO-67) coated with molecularly imprinted polymers (MOFs–MIPs) as a selective extraction phase.[172] The actual SERS-active substrate was a silver-coated copper sheet, while the MOFs–MIPs acted as a clean-up and enrichment layer, reducing matrix effects and concentrating the analyte. Although the LoD reached 3.6 nmol L^{-1}, which is not the lowest among reported systems, the sensor exhibited excellent selectivity, even in the presence of structurally similar pesticides. It also achieved high recovery rates ranging from 92.7% to 108.2% in real water samples.[172] This approach demonstrates how selective preconcentration can enhance SERS performance in complex matrices.

3.1.4.1. SERS reporters associated with biorecognition. However, the direct use of biorecognition results in a less intense SERS signal. To overcome this, reporter molecules conjugated with plasmonic materials can be used for indirect measurement. These compounds typically consist of small molecules with aromatic rings and SH groups, such as 4-aminothiophenol (4-ATP), 4-mercaptobenzoic acid (4-MBA), 4-mercaptobenzonitrile (4-MBN), and 4-nitrobenzenethiol (4-NBT). The presence of SH groups improves the binding with plasmonic nanoparticles (Au and Ag), and the aromatic ring is responsible for a characteristic spectral fingerprint.[169,173] To improve selectivity, highly selective target analyte-capture technologies, such as aptamers and antibody recognition, can be used. This approach is used not only for pesticides but also for clinical analysis.[28,104,105,173–176]

Xu *et al.* (2020) quantified 2,4 D using a SERS-tag (4-MBA) bound to Au@Ag nanoflowers and conjugated with the 2,4 D antigen (Au@Ag@MBA-antigen). The authors used a competitive strategy using a magnetic nanoparticle (MNP) conjugated

with the 2,4 D antibody to recognize the analyte. The author's approach is depicted in Fig. 10.[104]

The Au@Ag@MBA-antigen/antibody-MNPs complex demonstrated a robust SERS signal in the absence of 2,4 D pesticide due to the enhanced Au@Ag electromagnetic hot-spot effect. However, in the presence of the pesticide, the antibody bound to it instead of the Au@Ag@MBA-antigen, causing the Au@Ag@MBA-antigen to separate from the antibody-MNPs, which weakened the SERS signal. This weakened signal was attributed to the competition between the 2,4 D pesticide and antibody-MNPs for the Au@Ag@MBA-antigen. The authors achieved a LoD of 498 μmol L^{-1} and recovery values between 89.73% and 100.27% for the tea and milk samples.[104] Similarly, Sun *et al.* (2021) used the same strategy to quantify imidacloprid using a cuboid particle with Au nanorods (AuNRs) as the core and an Ag shell bound with 4-MBN as a SERS reporter conjugated with the imidacloprid antigen (AuNR@Ag-MBN-antigen). Fe_2O_3 MNPs were conjugated with the imidacloprid antibody. As discussed, both interact and conjugate when the Fe_2O_3-antibody is added to a solution containing the AuNR@Ag-MBN-antigen. The signal obtained from the MNP associated with the SERS reporter was very distinct. However, in a matrix with imidacloprid, the Fe_2O_3-antibody interacts with the analyte, impeding the formation of Fe_2O_3-antibody@AuNR@Ag-MBN-antigen. This strategy is known as competitive, and the authors reported a LoD of 9.58 nmol L^{-1} and recovery values of 96.8–100.5% for the apple juice and river water samples.[177]

Another promising method for detecting pesticides involves using aptamers conjugated to a SERS substrate as a recognition strategy. Aptamers are short synthetic single-stranded oligonucleotides that bind specifically to various molecular targets such as small molecules, proteins, and nucleic acids. Sun *et al.* (2019) developed an innovative approach for detecting and quantifying acetamiprid using a SERS aptasensor. They first prepared an AgNP@Si substrate and modified it with complementary DNA
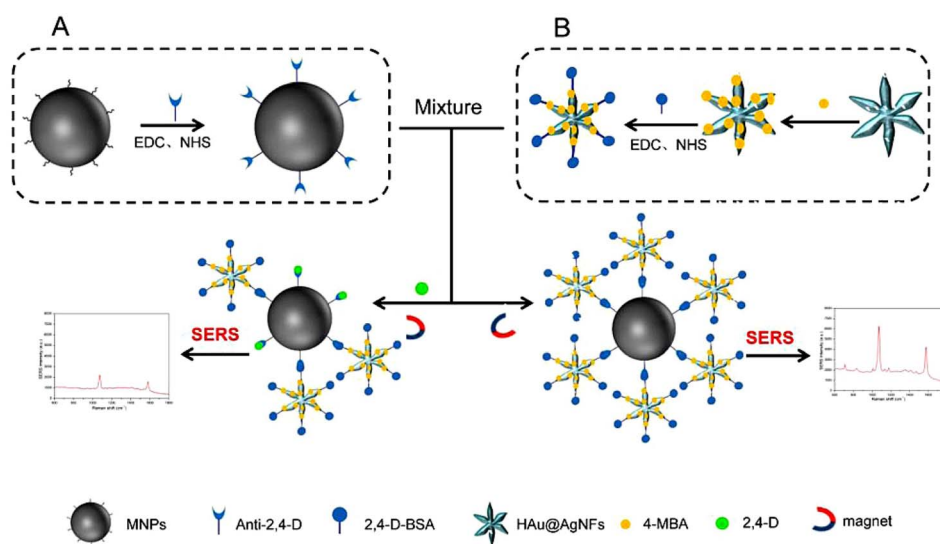

Fig. 10 Schematic illustration of the strategy used for 2,4-D analysis using an Au@Ag@MBA-antigen SERS-tag. (A) Functionalization of magnetic nanoparticles (MNPs) with anti-2,4-D for selective recognition. (B) Preparation of Au@Ag nanoflowers labeled with 4-MBA and conjugated with 2,4-D–BSA. This figure has been adapted/reproduced from ref. 104 with permission from Elsevier, copyright 2025.
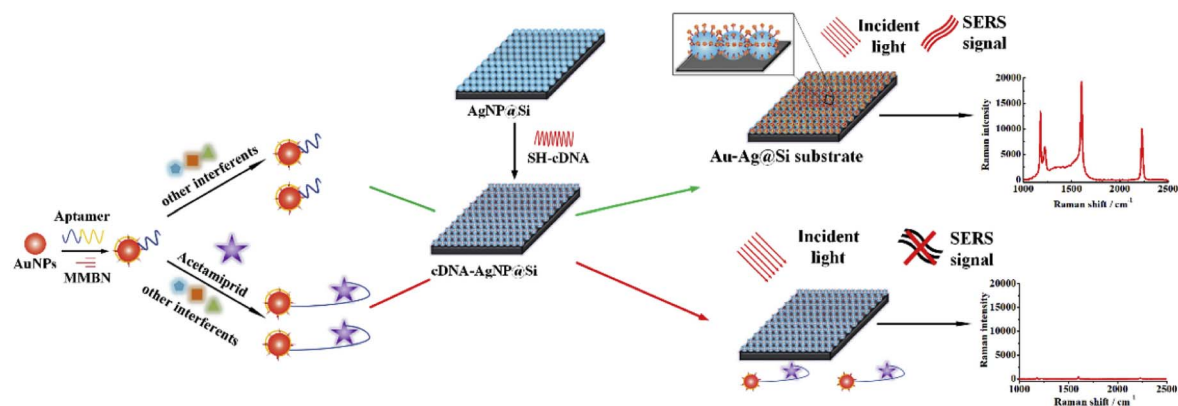
Fig. 11 Schematic of SERS aptasensor substrate fabrication and mechanism for acetamiprid detection. This figure has been adapted/reproduced from ref. 178 with permission from Elsevier, copyright 2025.

(cDNA). They then modified a solution of AuNPs with the SERS tag 4-(mercaptomethyl) benzonitrile (MMBN), which was bound to the target aptamer. The key aspect of this methodology is that acetamiprid molecules in the samples specifically bind to the aptamer, preventing the formation of the AuNPs@MMBN@aptamer-cDNA@AgNPs@Si hybrid through DNA sequence linking. The Raman signal intensity of MMBN in AuNPs@MMBN@aptamer-cDNA@AgNPs@Si decreased as the concentration of acetamiprid increased, as illustrated in Fig. 11. Using this approach, the authors achieved a LoD of 6.8 nmol L^{-1} and successfully quantified acetamiprid in apple juice samples, with recovery values ranging from 86.1% to 100.3%.[178]

Biorecognition elements such as antibodies, aptamers, and molecularly imprinted polymers introduce high molecular selectivity into SERS-based detection. Table 3 summarizes representative studies that leverage these strategies to achieve enhanced specificity in pesticide sensing.

3.1.5. Lateral flow immunochromatographic assay combined with SERS. Another noteworthy method is lateral flow immunochromatographic assays (LFAs or ICA), a cost-effective and paper-based solution for rapidly detecting target analytes in liquid samples. These assays rely on immunological reactions (antibodies) and chromatographic separation and have many applications, including pregnancy, virus, and pesticide detection.[35,185,186] However, they lack quantitative detection capabilities because of their reliance on visual read-outs.[187] Researchers have proposed alternative methods, such as fluorescence spectroscopy, electrochemistry, and chemiluminescence, but these face issues, such as photobleaching, and require extensive washing after incubation.[188]

Thus, the SERS approach enables the quantification of analytes in LFAs, overcoming the drawbacks mentioned earlier. In this manner, Li et al. (2019) combined LFA with a SERS tag to

Table 3 Overview of biorecognition-enhanced SERS sensors for pesticide analysis

| Biorecognition in SERS detection				
Pesticide	Samples	Substrate	Limit of detection	References
2, 4 D	Tea and milk	Au@Ag@MBA-antigen	498 µmol L^{-1}	104
Imidacloprid	Apple juice and river water	AuNR@Ag@MBA-antigen	9.58 nmol L^{-1}	177
Glyphosate	Soil	COF@AuNP@aptamer-VBB	0.002 nmol L^{-1}	105
Paraquat	Environmental water	Au@aptamer	0.10 µmol L^{-1}	170
Thiram	—	Au@MBA@AgNP	1.58 nmol L^{-1}	63
Thiabendazole	—	Au@MBA@AgNP	1.26 nmol L^{-1}	63
Fenthion	Seawater	AuNP@MIP	10 nmol L^{-1}	171
Chlorpyrifos	Cucumber, pear and river water	AuNP@PB-aptamer	0.066 ng mL^{-1}	179
Isocarbophos	Apple juice	Ag@MH-aptamer	3.4 µmol L^{-1}	180
Ornethoate	Apple juice	Ag@MH-aptamer	24 µmol L^{-1}	180
Phorate	Apple juice	Ag@MH-aptamer	0.4 µmol L^{-1}	180
Profenofos	Apple juice	Ag@MH-aptamer	14 µmol L^{-1}	180
Diazinon	Environmental water	UiO-67@MIP – Ag film	3.6 nmol L^{-1}	172
Methyl parathion	Apple peels	Ag@Au@MBA-aptamer	1.7 nmol L^{-1}	181
Acetamiprid		Au^{MBA}@Ag^{MBA}	0.27 µg kg^{-1}	
Carbendazim		Au^{MBA}@Ag^{MBA}	1.71 µg kg^{-1}	
Malathion	Cereals	Tb-MOF@Au@MIP	0.06 ng mL^{-1}	182
Diazinon	Wastewater and soil	Ag@ICNPs-aptamer	0.53 nmol L^{-1}	183
Kanamycin	Milk	Au@Ag@MBA-aptamer	142 pg mL^{-1}	184
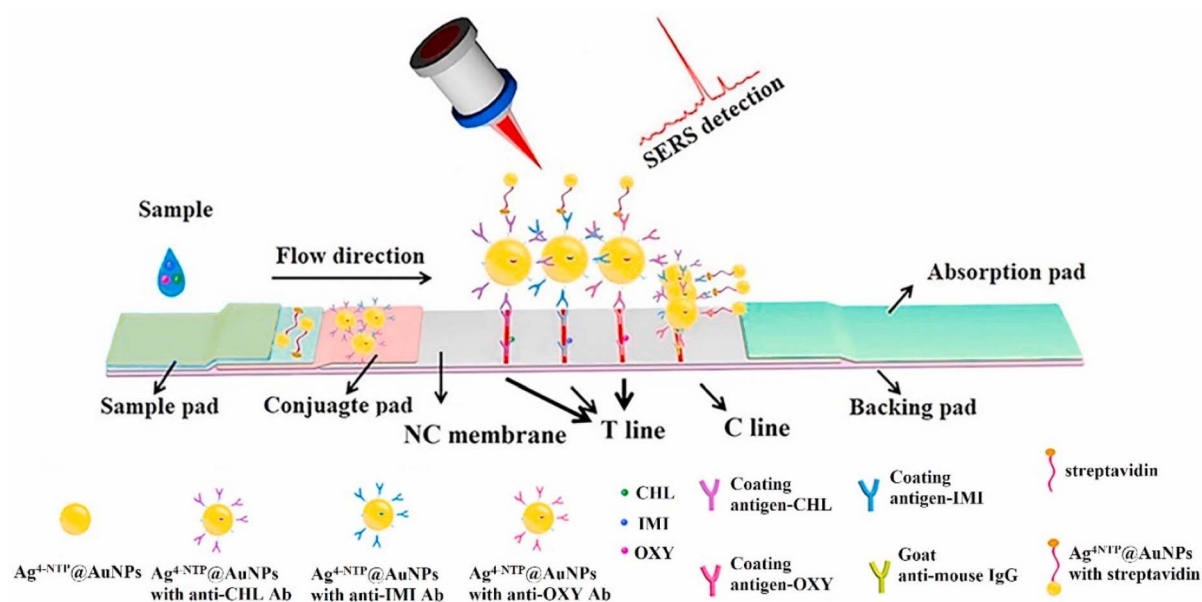
Fig. 12 Scheme of the LFA-SERS strategy using enhanced Ag$^{4\text{-NTP}}$@Au for the multiplex strip. This figure has been adapted/reproduced from ref. 189 with permission from Elsevier, copyright 2025.

quantify cypermethrin and esfenvalerate. They used 4-ATP and 4-MBA as Raman reporters, immobilizing them on the test line of the LFA strip to facilitate SERS measurements. The simultaneous dual detection method involved immobilizing the two test lines using antibodies specifically designed to detect each of the targeted pesticides. The LoDs of the LFA-SERS system were 0.55 and 0.062 fmol L^{-1} for cypermethrin and esfenvalerate, respectively.[188] A study by Sheng *et al.* (2021) presented another LFA-SERS assay for the analysis of chlorothalonil, imidacloprid, and oxyfluorfen pesticides. In this study, the authors used 4-NTP as a reporter and Ag@Au nanoparticles conjugated with antibodies specific to the analytes, as depicted in Fig. 12. The developed LFA-SERS strip achieved LoDs of 0.564, 3.91, and 5.68 nmol L^{-1} for chlorothalonil, imidacloprid, and oxyfluorfen, respectively.[189]

Dong *et al.* (2024) used LFA-SERS to quantify triadimefon fungicides. The test line of the LFA-SERS strip consists of Au@Ag with a 5,5-dithiobis-(2-nitrobenzoic acid) (DTNB) Raman reporter embedded into the core–shell structure and bound to the triadimefon antibody. This sensor achieved a LoD of 14.9 μmol L^{-1} and recovery values of 88.53–117.13% for cucumber and tobacco samples.[190] Moreover, Wang *et al.* (2024) developed LFA-SERS for the dual detection of carbendazim and imidacloprid. The first test line consisted of AuNPs modified with Prussian blue and the carbendazim antibody, and the second test line consisted of AuNPs conjugated with 4-MBA and the imidacloprid antibody. The authors achieved a LoD of 105 and 78 nmol L^{-1} for carbendazim and imidacloprid, respectively, and successfully tested cucumber, apple, and lake water samples, obtaining recovery values ranging from 85.83% to

Table 4 Recent applications of LFA–SERS platforms for pesticide detection

LFA-SERS

Pesticide	Samples	Substrate	Limit of detection	References
Cypermethrin	Milk, tap water, and river water	Au@MBA-antibody	0.55 fmol L^{-1}	188
Esfenvalerate	Milk, tap water, and river water	Au@ATP-antibody	0.062 fmol L^{-1}	188
Chlorothalonil	Soil and rice samples	Ag@Au@NTP-antibody	0.564 nmol L^{-1}	189
Imidacloprid	Soil and rice samples	Ag@Au@NTP-antibody	3.91 nmol L^{-1}	189
Oxyfluorfen	Soil and rice samples	Ag@Au@NTP-antibody	5.68 nmol L^{-1}	189
Acetamiprid	Apple and orange	Au^{MBA}@Ag^{MBA}-antibody	0.27 μg kg^{-1}	194
Carbendazim	Apple and orange	Au^{MBA}@Ag^{MBA}-antibody	1.71 μg kg^{-1}	194
Triadimefon	Cucumber and tobacco	Au@Ag@DTNB-antibody	14.9 μmol L^{-1}	190
Carbendazim	Cucumber, apple, and lake water	AuNP@PB-antibody	105 nmol L^{-1}	191
Imidacloprid	Cucumber, apple, and lake water	AuNP@MBA-antibody	78 nmol L^{-1}	191
Phorate	Celery	Fe$_3$O$_4$@AuNP@DTNB-antibody	1.0 ng mL^{-1}	192
Fipronil	Cucumber and apple juice	Bimetallic Au@Ag@Ag nanorods	256 fg mL^{-1}	195
Carbofuran	Apple, cucumber and cabbage	Au@Ag@DTNB-antibody	0.45 pmol L^{-1}	193

116.53%.[191] Li *et al.* (2024) developed a MNP covered with AuNPs, labeled with DTNB and conjugated with the antibody for phorate pesticide. This Fe_3O_4@AuNP@DTNB-antibody probe was successfully used in LFA-SERS strips with a LoD of 1.0 ng mL^{-1}, in accordance with the local legislation. The authors validated the methodology of analyzing phorate in celery samples with good recovery values (96.7–105.1%).[192] Pei *et al.* (2024) used a core–shell Au@Ag structure labeled with DTNB and an antibody for carbofuran detection on the test line of an LFA-SERS strip. The authors achieved a LoD of 0.45 pmol L^{-1}, and quantified the carbofuran pesticide in apple, cucumber, and cabbage samples with recovery values of 92.65–112.4%.[193]

LFAs combined with SERS readout offer a powerful strategy for rapid and on-site pesticide detection, integrating the simplicity of immunochromatography with the sensitivity of plasmonic enhancement. Table 4 presents recent applications of LFA–SERS systems, highlighting their analytical capabilities and suitability for field deployment.

The integration of LFA with SERS represents a pivotal advancement in pesticide detection, effectively merging the high selectivity of antibody-based recognition with the exceptional sensitivity of plasmon-enhanced Raman scattering. This hybrid approach addresses the inherent limitations of conventional LFA, enabling quantitative analysis at ultra-low concentrations. The use of well-defined SERS reporters, such as 4-MBA, 4-ATP, 4-NTP, and DTNB, combined with plasmonic nanostructures (*e.g.*, AuNPs, Au@Ag, and Fe_3O_4@AuNPs), ensures the generation of intense and reproducible Raman signals at the test line. As demonstrated in recent studies, this synergistic combination consistently yields detection limits down to the femtogram per milliliter range, establishing LFA–SERS as one of the most sensitive and field-deployable platforms for rapid pesticide screening.

4. What influences detection limits in SERS for pesticides?

While the variety of substrates and approaches demonstrates promising capabilities for pesticide detection, reported LoDs vary significantly across studies for the same analytes. Understanding the sources of these discrepancies is crucial for advancing the field, and some factors can influence this LoD variability. These discrepancies, often spanning multiple orders of magnitude, complicate direct comparison of sensor performance and hinder the identification of optimal substrates and protocols. To elucidate the reasons behind such variations, it is crucial to understand the substrate fabrication techniques, sample pretreatment, LoD calculation methodologies, and analyte–substrate interactions.

The morphology, composition, and fabrication method of SERS substrates profoundly impact the local electromagnetic enhancement and hotspot distribution, which are crucial for sensitivity, as discussed before. Advanced nanostructures, such as core–shell hybrids, hierarchical assemblies, and metal–semiconductor composites, generally yield higher enhancement factors compared to simpler colloidal films or unstructured metal surfaces. For example, substrates employing Ag nanowires or nanostars often provide denser hotspots than drop-cast nanoparticle aggregates, resulting in lower LoDs. Variability in synthesis conditions (*e.g.*, particle size, shape uniformity, and surface chemistry) further affects reproducibility and signal strength, contributing to inconsistent LoDs reported for the same pesticide.[60,67,71,72,196–198]

Sample preparation influences analyte availability and matrix effects, which significantly affect SERS signal intensity and reproducibility. Pretreatment methods such as QuEChERS extraction, filtration, centrifugation, or swabbing help improve analyte concentration and reduce interference from complex sample matrices (*e.g.*, food, biological fluids, or environmental water).[199] These steps are especially crucial because, in real-world samples, the Raman signal of the target pesticide are often overlapped or masked by background signals from other coexisting substances, hindering accurate detection. Inconsistent or absent pretreatment can lead to poor analyte adsorption on SERS-active sites, increased noise, and ultimately elevated reported LoDs. Therefore, standardizing sample preparation protocols is essential to ensure reproducibility and enable meaningful comparison across studies. To further enhance selectivity and minimize matrix interference, bio-recognition strategies such as aptamer binding, antigen–antibody interactions, and molecularly imprinted polymers (MIPs) are increasingly integrated into SERS platforms.[200,201] These strategies provide molecular specificity and will be discussed in more detail below.

To obtain a sensitive substrate, it is essential to understand the chemical affinity between pesticide molecules and the substrate surface, since it plays a pivotal role in SERS sensitivity by influencing both EM and CM.[22,202] Molecules containing sulfur or thiol functional groups, such as thiram, exhibit strong chemisorption with noble metals like Ag and Au, resulting in robust signal enhancement and lower LoDs.[28,203] Conversely, analytes lacking such direct binding groups may rely more on weaker interactions such as π–π stacking, electrostatic attraction, or charge transfer, particularly when adsorbed onto graphene-based or semiconductor-modified substrates.[204]

Overall, the use of thiram exemplifies how analyte–substrate interactions directly govern SERS performance. It can be considered a pesticide probe molecule, due to its strong interactions with plasmonic metal surfaces. The wide range of reported LoDs underscores the influence of substrate design, surface chemistry, functionalization strategies, and recognition-driven selectivity. These findings highlight the importance of tailoring substrates not only for enhancing efficiency but also for target-specific interaction, particularly for field applications requiring reproducibility and high sensitivity in complex matrices.

5. Challenges associated with SERS

SERS application in pesticide detection faces numerous challenges. Achieving a LoD and a linear range that complies with regulatory MRLs is a primary obstacle, with many studies failing to meet these standards. The absence of detailed protocols for

sample processing and pre-treatment, including grinding, extraction solutions, filtration, centrifugation, and cleaning, restricts effective *in situ* analysis. Moreover, validating SERS accuracy and reliability in actual samples is crucial but often neglected. Ensuring high reproducibility, repeatability, selectivity, and scalability is vital for broader adoption, yet many studies ignore these aspects. Moreover, it is crucial to consider the stability and shelf life of SERS substrates for practical use. However, there is often a lack of long-term performance and storage data, which hinders comprehensive evaluation.

Additionally, reliance on costly bench-top Raman spectrometers restricts SERS practicality for on-site and real-time analysis. Developing methodologies with portable Raman spectrometers would democratize SERS, making it more accessible for agricultural, food safety, and environmental monitoring.[31] Addressing these issues through improved detection limits, standardized protocols, and portable equipment is critical for advancing SERS as a robust pesticide detection method.

6. Economic viability

Beyond material innovations, economic feasibility governs real-world deployment. In this sense, the financial feasibility of SERS for pesticide detection is critical, yet many studies overlook substrate and analysis costs, creating a gap in understanding its practical implementation. The development and adoption of SERS are hindered by the limited availability and high cost of commercial substrates. For example, Metrohm® charges $425 for 25 paper-based substrates, Stellarnet® sells 25 units for $250, Simelco® offers five Ag and Au silicon-based substrates for €350, and Oceanoptics® provides five Ag and Au glass substrates for $90.[205–208] These prices limit accessibility and practicality for routine use, as substrates are often single-use. Additionally, the high cost of Raman spectrometers further restricts the adoption of SERS technology to well-funded labs. Addressing these challenges requires extensive research into mass-producing SERS substrates with cost-effective methods to ensure high quality and reproducibility. Lowering substrate costs would enhance SERS's affordability and practicality, making this analytical technique suitable for routine pesticide detection and accessible to a broader range of applications.

7. Future directions

The future of SERS technology in pesticide detection is promising but requires advancements in several key areas to enhance its applicability and effectiveness. Improving SERS selectivity and sensitivity is essential and achievable through novel substrates that offer higher enhancement and better reproducibility. Additionally, conjugating antibodies or aptamers with reporter molecules can significantly enhance selectivity, enabling specific detection of target pesticides in complex matrices. Another promising direction is multiplexed SERS for detecting several agrochemicals simultaneously. Although quantitative analysis in food samples is still challenging, the LFA-SERS hybrid approach can provide qualitative and quantitative information on multiple analytes, combining the low cost, simplicity, rapid detection, and selectivity of LFA with the high sensitivity of SERS, making it ideal for comprehensive pesticide analysis. Simplifying sample processing is also crucial. Developing easy sample pre-treatment protocols will make SERS more practical for real-world applications, particularly *in situ* analysis, and reduce time and costs.

Addressing the trade-off between substrate reusability and signal fidelity is essential for practical SERS applications. It is necessary to develop strategies that minimize analyte degradation and substrate alteration caused by repeated laser exposure, such as optimizing laser parameters and designing more robust photocatalytic materials. These efforts will be critical for achieving reliable and sustainable pesticide detection across multiple reuse cycles.

Another transformative direction for advancing SERS-based pesticide detection lies in the integration of artificial intelligence (AI) across the entire analytical procedure.[209] AI has demonstrated remarkable capability in extracting high-level features from complex spectral datasets, identifying subtle patterns that may be imperceptible to human analysts, and significantly improving the accuracy and reliability of detection.[209–211] In the context of pesticide analysis, AI can facilitate spectral preprocessing, noise reduction, baseline correction, and multivariate classification, enabling robust identification even in complex food and environmental matrices. Furthermore, AI-driven models such as convolutional neural networks and large Raman models trained on extensive spectral databases can support multiplexed detection, enhance reproducibility, and guide substrate optimization by predicting structure–property relationships.[211] As such, the convergence of AI and SERS opens new avenues for real-time, *in situ* monitoring with minimal human intervention, paving the way for innovative, adaptive sensing platforms. Nonetheless, advancing toward AI-driven rather than merely AI-assisted SERS requires careful attention to data quality, standardization, interpretability, and ethical considerations to ensure transparency, fairness, and broad acceptance in practical applications.[209–211] Moreover, integrating AI with SERS technology represents a frontier for efficient result delivery.[175,212] Addressing these areas can make SERS a more robust, reliable, and widely accessible tool for ensuring food and environmental safety.

8. Conclusions

In conclusion, this study discusses the use of SERS for pesticide analysis, highlighting new approaches and the advantages and disadvantages of the technique. The future of SERS technology lies in making it more affordable, portable, and versatile. By addressing the current limitations in substrate availability, cost, and equipment portability, SERS can become a standard tool for many applications, including clinical diagnostics, food analysis and environmental monitoring.

Author contributions

Gabriel F. S. dos Santos: writing – original draft, writing – review & editing; visualization, formal analysis, investigation;

Giordano T. Paganoto: writing – review & editing, formal analysis, investigation; Lucas C. Cosme: writing – review & editing, formal analysis, investigation; Adilson R. Prado: writing – review & editing, investigation; Sérvio Túlio A. Cassini: writing – review & editing, funding acquisition; Marco C. C. Cunegundes: writing – review & editing, funding acquisition; Jairo P. Oliveira: conceptualization, writing – review & editing, project administration, supervision.

Conflicts of interest

The authors declare that they have no known competing financial interests or personal relationships that could have appeared to influence the work reported in this paper.

Data availability

No primary research results, software or code have been included and no new data were generated or analysed as part of this review.

Acknowledgements

References

1 FAO, IFAD, UNICEF, WFP and WHO, *The State of Food Security and Nutrition in the World 2023, Rome*, 2023.

2 FAO, *Pest and pesticide management*, **https://www.fao.org/pest-and-pesticide-management/en/**.

3 World Health Organization, *A guide to healthy food markets*, **https://iris.who.int/handle/10665/43393**.

4 World Health Organization, Food safety, **https://www.who.int/news-room/fact-sheets/detail/food-safety**.

5 M. Tudi, H. Daniel Ruan, L. Wang, J. Lyu, R. Sadler, D. Connell, C. Chu and D. T. Phung, *Int. J. Environ. Res. Public Health*, 2021, **18**, 1112.

6 U. Asghar, M. F. Malik and A. Javed, *J. Ecosys. Ecograph*, 2016, **s5**, 005.

7 M. C. O. Souza, J. C. Cruz, C. A. Cesila, N. Gonzalez, B. A. Rocha, J. A. Adeyemi, M. Nadal, J. L. Domingo and F. Barbosa, *Environ. Res.*, 2023, **228**, 115811.

8 P. Nicolopoulou-Stamati, S. Maipas, C. Kotampasi, P. Stamatis and L. Hens, *Front. Public Heal.*, 2016, **4**, 1–8.

9 Y. Jin, L. Wang, G. Chen, X. Lin, W. Miao and Z. Fu, *Environ. Toxicol. Pharmacol.*, 2014, **37**, 782–790.

10 J. George, S. Prasad, Z. Mahmood and Y. Shukla, *J. Proteomics*, 2010, **73**, 951–964.

11 C. E. Handford, C. T. Elliott and K. Campbell, *Integr. Environ. Assess. Manag.*, 2015, **11**, 525–536.

12 D. Orazbayeva, A. Muratuly, M. Bektassov, A. Zhakupbekova and B. Kenessov, *Trends Environ. Anal. Chem.*, 2022, **35**, e00174.

13 I. S. Belmonte, T. M. Pizzolato and M. R. Gama, *Trends Environ. Anal. Chem.*, 2022, **35**, e00171.

14 X. Song, F. Li, T. Yan, F. Tian, L. Ren, C. Jiang, Q. Wang and S. Zhang, *Process Saf. Environ. Prot.*, 2022, **165**, 610–622.

15 J. Aspromonte, C. Lancioni and G. Purcaro, *Methods Protoc.*, 2022, **5**, 82.

16 S. N. Sinha, R. Ungarala, D. Kumar, R. Sangaraju and S. Kumar, *PLoS One*, 2022, **17**, 1–16.

17 J. Yi, E.-M. You, R. Hu, D.-Y. Wu, G.-K. Liu, Z.-L. Yang, H. Zhang, Y. Gu, Y.-H. Wang, X. Wang, H. Ma, Y. Yang, J.-Y. Liu, F. R. Fan, C. Zhan, J.-H. Tian, Y. Qiao, H. Wang, S.-H. Luo, Z.-D. Meng, B.-W. Mao, J.-F. Li, B. Ren, J. Aizpurua, V. A. Apkarian, P. N. Bartlett, J. Baumberg, S. E. J. Bell, A. G. Brolo, L. E. Brus, J. Choo, L. Cui, V. Deckert, K. F. Domke, Z.-C. Dong, S. Duan, K. Faulds, R. Frontiera, N. Halas, C. Haynes, T. Itoh, J. Kneipp, K. Kneipp, E. C. Le Ru, Z.-P. Li, X. Y. Ling, J. Lipkowski, L. M. Liz-Marzán, J.-M. Nam, S. Nie, P. Nordlander, Y. Ozaki, R. Panneerselvam, J. Popp, A. E. Russell, S. Schlücker, Y. Tian, L. Tong, H. Xu, Y. Xu, L. Yang, J. Yao, J. Zhang, Y. Zhang, Y. Zhang, B. Zhao, R. Zenobi, G. C. Schatz, D. Graham and Z.-Q. Tian, *Chem. Soc. Rev.*, 2025, **54**, 1453–1551.

18 S. Schlücker, *Angew. Chem., Int. Ed.*, 2014, **53**, 4756–4795.

19 J. Langer, D. J. de Aberasturi, J. Aizpurua, R. A. Alvarez-Puebla, B. Auguié, J. J. Baumberg, G. C. Bazan, S. E. J. Bell, A. Boisen, A. G. Brolo, J. Choo, D. Cialla-May, V. Deckert, L. Fabris, K. Faulds, F. Javier García de Abajo, R. Goodacre, D. Graham, A. J. Haes, C. L. Haynes, C. Huck, T. Itoh, M. Käll, J. Kneipp, N. A. Kotov, H. Kuang, E. C. Le Ru, H. K. Lee, J. F. Li, X. Y. Ling, S. A. Maier, T. Mayerhöfer, M. Moskovits, K. Murakoshi, J. M. Nam, S. Nie, Y. Ozaki, I. Pastoriza-Santos, J. Perez-Juste, J. Popp, A. Pucci, S. Reich, B. Ren, G. C. Schatz, T. Shegai, S. Schlücker, L. L. Tay, K. George Thomas, Z. Q. Tian, R. P. van Duyne, T. Vo-Dinh, Y. Wang, K. A. Willets, C. Xu, H. Xu, Y. Xu, Y. S. Yamamoto, B. Zhao and L. M. Liz-Marzán, *ACS Nano*, 2020, **14**, 28–117.

20 R. Panneerselvam, G. K. Liu, Y. H. Wang, J. Y. Liu, S. Y. Ding, J. F. Li, D. Y. Wu and Z. Q. Tian, *Chem. Commun.*, 2017, **54**, 10–25.

21 R. S. Das and Y. K. Agrawal, *Vib. Spectrosc.*, 2011, **57**, 163–176.

22 P. Mosier-Boss, *Nanomaterials*, 2017, **7**, 142.

23 M. Feizpour, Q. Liu, T. Van der Donck, H. Thienpont, W. Meulebroeck and H. Ottevaere, *J. Phys. Photonics*, 2024, **6**, 025002.

24 L. Ouyang, W. Ren, L. Zhu and J. Irudayaraj, *Rev. Anal. Chem.*, 2016, **36**(1), DOI: **10.1515/revac-2016-0027**.

25 X. Lin, F. Lei, X. Liang, Y. Jiao, X. Zhao, Z. Li, C. Zhang and J. Yu, *Opto-Electronic Adv.*, 2025, **8**, 240260.

26 H. Qin, S. Zhao, H. Gong, Z. Yu, Q. Chen, P. Liang and D. Zhang, *Biosensors*, 2023, **13**, 479.

27 T. Wang, S. Wang, Z. Cheng, J. Wei, L. Yang, Z. Zhong, H. Hu, Y. Wang, B. Zhou and P. Li, *Chem. Eng. J.*, 2021, **424**, 130323.

28 R. Moldovan, B.-C. Iacob, C. Farcău, E. Bodoki and R. Oprean, *Nanomaterials*, 2021, **11**, 304.

29 C. Liu, D. Xu, X. Dong and Q. Huang, *Trends Food Sci. Technol.*, 2022, **128**, 90–101.

30 L. Jiang, M. M. Hassan, S. Ali, H. Li, R. Sheng and Q. Chen, *Trends Food Sci. Technol.*, 2021, **112**, 225–240.

31 R. Pilot, *J. Raman Spectrosc.*, 2018, **49**, 954–981.

32 S. Y. Wang, X. C. Shi, G. Y. Zhu, Y. J. Zhang, D. Y. Jin, Y. D. Zhou, F. Q. Liu and P. Laborda, *Trends Food Sci. Technol.*, 2021, **116**, 583–602.

33 L. Liu, Y. Wang, Z. Xue, B. Peng, X. Kou and Z. Gao, *Trends Food Sci. Technol.*, 2024, **148**, 104487.

34 J. Budd, B. S. Miller, N. E. Weckman, D. Cherkaoui, D. Huang, A. T. Decruz, N. Fongwen, G.-R. Han, M. Broto, C. S. Estcourt, J. Gibbs, D. Pillay, P. Sonnenberg, R. Meurant, M. R. Thomas, N. Keegan, M. M. Stevens, E. Nastouli, E. J. Topol, A. M. Johnson, M. Shahmanesh, A. Ozcan, J. J. Collins, M. Fernandez Suarez, B. Rodriguez, R. W. Peeling and R. A. McKendry, *Nat. Rev. Bioeng.*, 2023, **1**, 13–31.

35 M. D. L. Jara, L. A. C. Alvarez, M. C. C. Guimarães, P. W. P. Antunes and J. P. de Oliveira, *Environ. Sci. Pollut. Res.*, 2022, **29**, 46487–46508.

36 Q. Zhang, L. Fang, B. Jia, N. Long, L. Shi, L. Zhou, H. Zhao and W. Kong, *TrAC Trends Anal. Chem.*, 2021, **144**, 116427.

37 M. Fleischmann, P. J. Hendra and A. J. McQuillan, *Chem. Phys. Lett.*, 1974, **26**, 163–166.

38 D. L. Jeanmaire and R. P. Van Duyne, *J. Electroanal. Chem. Interfacial Electrochem.*, 1977, **84**, 1–20.

39 M. G. Albrecht and J. A. Creighton, *J. Am. Chem. Soc.*, 1977, **99**, 5215–5217.

40 M. Moskovits, *J. Chem. Phys.*, 1978, **69**, 4159–4161.

41 J. Gersten and A. Nitzan, *J. Chem. Phys.*, 1980, **73**, 3023–3037.

42 M. Moskovits, *Solid State Commun.*, 1979, **32**, 59–62.

43 H. Metiu and P. Das, *Annu. Rev. Phys. Chem.*, 1984, **35**, 507–536.

44 G. C. Schatz, *Acc. Chem. Res.*, 1984, **17**, 370–376.

45 T. Itoh, M. Procházka, Z.-C. Dong, W. Ji, Y. S. Yamamoto, Y. Zhang and Y. Ozaki, *Chem. Rev.*, 2023, **123**, 1552–1634.

46 X. Wang, Y. Mao and Z. Wang, *ChemElectroChem*, 2024, **11**(8), DOI: 10.1002/celc.202300805.

47 C. F. Bohren and D. R. Huffman, *Absorption and Scattering of Light by Small Particles*, Wiley, 1998.

48 K. Kneipp, M. Moskovits and H. Kneipp, *Surface-Enhanced Raman Scattering*, Springer Berlin Heidelberg, 2006, vol. 103.

49 H. Ma, S.-Q. Pan, W.-L. Wang, X. Yue, X.-H. Xi, S. Yan, D.-Y. Wu, X. Wang, G. Liu and B. Ren, *ACS Nano*, 2024, **18**, 14000–14019.

50 D. J. Trivedi, B. Barrow and G. C. Schatz, *J. Chem. Phys.*, 2020, **153**(12), DOI: 10.1063/5.0023359.

51 I. Chaudhry, G. Hu, H. Ye and L. Jensen, *ACS Nano*, 2024, **18**, 20835–20850.

52 E. C. Le Ru and B. Auguié, *ACS Nano*, 2024, **18**, 9773–9783.

53 M. B. Bhavya, R. Prabhu B., B. M. Shenoy, P. Bhol, S. Swain, M. Saxena, N. S. John, G. Hegde and A. K. Samal, *Environ. Sci. Nano*, 2020, **7**, 3999–4009.

54 R. B. Rashid, A. M. Alwan and M. Q. Zayer, *Appl. Phys. A*, 2025, **131**, 392.

55 A. Afroozeh, *Plasmonics*, 2024, **20**, 63–81.

56 Y. Wan, Q. Wei, H. Sun, H. Wu, Y. Zhou, C. Bi, J. Li, L. Li, B. Liu, D. Wang, X. Wang, C. Wang and W. Liu, *Chem. Eng. J.*, 2025, **507**, 160813.

57 M. Jin, H. Pan, G. Gao, M. Zhang, H. Wei, X. Meng, W. Chen, X. Zhang, M. Shang and C. Wang, *Chem. Eng. J.*, 2025, **518**, 164800.

58 H. Wei and H. Xu, *Nanoscale*, 2013, **5**, 10794.

59 H. Ko, S. Singamaneni and V. V. Tsukruk, *Small*, 2008, **4**, 1576–1599.

60 T. Y. Jeon, D. J. Kim, S.-G. Park, S.-H. Kim and D.-H. Kim, *Nano Converg.*, 2016, **3**, 18.

61 R. Wang, S. Qiao, Y. He and Y. Ma, *Opto-Electronic Adv.*, 2025, **8**, 240275.

62 M. Magdy, *Plasmonics*, 2023, **18**, 803–809.

63 K. Wang and J. Li, *Sens. Actuators, B*, 2021, **263**, 120218.

64 D.-Y. Lin, C.-Y. Yu, C.-A. Ku and C.-K. Chung, *Micromachines*, 2023, **14**, 1343.

65 W. Wei, Y. Du, L. Zhang, Y. Yang and Y. Gao, *J. Mater. Chem. C*, 2018, **6**, 8793–8803.

66 K. Daoudi, M. Gaidi, S. Columbus, M. Shameer and H. Alawadhi, *Mater. Sci. Semicond. Process.*, 2022, **138**, 106288.

67 R. Shi, X. Liu and Y. Ying, *J. Agric. Food Chem.*, 2018, **66**, 6525–6543.

68 V. Suresh and F. L. Yap, *RSC Adv.*, 2015, **5**, 61671–61677.

69 R. Pilot, R. Signorini and L. Fabris, in *Metal Nanoparticles and Clusters*, Springer International Publishing, Cham, 2018, pp. 89–164.

70 C. Li, Y. Huang, X. Li, Y. Zhang, Q. Chen, Z. Ye, Z. Alqarni, S. E. J. Bell and Y. Xu, *J. Mater. Chem. C*, 2021, **9**, 11517–11552.

71 X. Tian, B. Zhang, L. Song, J. Bao, J. Yang, L. Sun, H. Pei and C. Song, *Batter. Energy*, 2025, **4**(4), DOI: 10.1002/bte2.20240053.

72 B.-X. Wang, G. Duan, W. Xu, C. Xu, J. Jiang, Z. Yang, Y. Wu and F. Pi, *Crit. Rev. Food Sci. Nutr.*, 2024, **64**, 472–516.

73 J. R. Lombardi and R. L. Birke, *J. Phys. Chem. C*, 2008, **112**, 5605–5617.

74 D. Grasseschi and H. E. Toma, *Coord. Chem. Rev.*, 2017, **333**, 108–131.

75 M. Muniz-Miranda, F. Muniz-Miranda, M. C. Menziani and A. Pedone, *Molecules*, 2023, **28**, 573.

76 A. Zozulya, A. Zyubin and I. Samusev, *R. Soc. Open Sci.*, 2025, **12**(6), DOI: 10.1098/rsos.242000.

77 C. Cappelli, S. Corni and J. Tomasi, *J. Chem. Phys.*, 2001, **115**, 5531–5535.

78 S. Jin, D. Zhang, B. Yang, S. Guo, L. Chen and Y. M. Jung, *Analyst*, 2024, **149**, 11–28.

79 R. Ozdemir, K. Ozkan Hukum, H. Usta and G. Demirel, *J. Mater. Chem. C*, 2024, **12**, 15276–15309.

80 J. M. Luther, P. K. Jain, T. Ewers and A. P. Alivisatos, *Nat. Mater.*, 2011, **10**, 361–366.

81 J. R. Lombardi and R. L. Birke, *J. Phys. Chem. C*, 2014, **118**, 11120–11130.

82 W. Ji, L. Li, J. Guan, M. Mu, W. Song, L. Sun, B. Zhao and Y. Ozaki, *Adv. Opt. Mater.*, 2021, **9**(24), DOI: **10.1002/adom.202101866**.

83 Y. Wang, M. Li, D. Wang, C. Han, J. Li, C. Wu and K. Xu, *Colloid Interface Sci. Commun.*, 2020, **39**, 100324.

84 L. Yang, Y. Yang, Y. Ma, S. Li, Y. Wei, Z. Huang and N. V. Long, *Nanomaterials*, 2017, **7**, 398.

85 C. Ye, Z. Zhu, X. Li, H. Zhou, M. Zhang, L. Yan, Z. Chen, Y. Huang and Y. Wu, *J. Alloys Compd.*, 2022, **901**, 163675.

86 S. Adesoye and K. Dellinger, *Sens. Bio-Sensing Res.*, 2022, **37**, 100499.

87 X. Ling and J. Zhang, *Small*, 2010, **6**, 2020–2025.

88 X. Ling, L. G. Moura, M. A. Pimenta and J. Zhang, *J. Phys. Chem. C*, 2012, **116**, 25112–25118.

89 T. You, N. Yang, Y. Shu and P. Yin, *J. Raman Spectrosc.*, 2019, **50**, 1510–1518.

90 Y. Xie, *Chemosensors*, 2022, **10**, 507.

91 D. You, R. Wang, J. Xie, L. Liu, K. Li, X. Han, T. Guo and C. Xu, *J. Mater. Chem. A*, 2022, **10**, 14078–14089.

92 Y. Wu, T. Sun, M. Shao, C. Ji, C. Li, C. Zhang and Z. Li, *Laser Photon. Rev.*, 2024, **19**(4), DOI: **10.1002/lpor.202401152**.

93 T. T. Tran, X. H. Vu, T. L. Ngo, T. T. H. Pham, D. D. Nguyen and V. D. Nguyen, *Phys. Chem. Chem. Phys.*, 2023, **25**, 15941–15952.

94 X. Tang, X. Fan, L. Yao, G. Li, M. Li, X. Zhao, Q. Hao and T. Qiu, *J. Phys. Chem. Lett.*, 2022, **13**, 7816–7823.

95 F. Tian, F. Bonnier, A. Casey, A. E. Shanahan and H. J. Byrne, *Anal. Methods*, 2014, **6**, 9116–9123.

96 Z. Wang, S. Wu, L. Colombi Ciacchi and G. Wei, *Analyst*, 2018, **143**, 5074–5089.

97 Z. Guo, X. Wu, H. Jayan, L. Yin, S. Xue, H. R. El-Seedi and X. Zou, *Food Chem.*, 2024, **434**, 137469.

98 A. M. Dowgiallo and D. A. Guenther, *J. Agric. Food Chem.*, 2019, **67**, 12642–12651.

99 Y. Wei, M. Qin, Y. Liu, X. Jia, J. Zhou and G. Wang, *J. Phys. Conf. Ser.*, 2025, **2961**, 012006.

100 J. Tang, W. Chen and H. Ju, *Sens. Actuators, B*, 2019, **287**, 576–583.

101 X. Li, G. Chen, L. Yang, Z. Jin and J. Liu, *Adv. Funct. Mater.*, 2010, **20**, 2815–2824.

102 D. Zhang, P. Liang, J. Ye, J. Xia, Y. Zhou, J. Huang, D. Ni, L. Tang, S. Jin and Z. Yu, *Anal. Bioanal. Chem.*, 2019, **411**, 7187–7196.

103 Y. Ma, Y. Wang, Y. Luo, H. Duan, D. Li, H. Xu and E. K. Fodjo, *Anal. Methods*, 2018, **10**, 4655–4664.

104 Y. Xu, F. Y. H. Kutsanedzie, M. M. Hassan, J. Zhu, H. Li and Q. Chen, *Sens. Actuators, B*, 2020, **324**, 128718.

105 Q. Liu, R. Zhang, B. Yu, A. Liang and Z. Jiang, *Sens. Actuators, B*, 2021, **344**, 130288.

106 L. Mikac, I. Rigó, M. Škrabić, M. Ivanda and M. Veres, *Molecules*, 2022, **27**, 5767.

107 S. K. Satani, S. S. B. Moram and V. R. Soma, *J. Phys. D Appl. Phys.*, 2023, **56**, 375103.

108 L. Jiang, K. Gu, R. Liu, S. Jin, H. Wang and C. Pan, *SN Appl. Sci.*, 2019, **1**, 627.

109 H. Yu, D. Guo, H. Zhang, X. Jia, L. Han and W. Xiao, *Spectrochim. Acta, Part A*, 2023, **285**, 121930.

110 T. Xie, Z. Cao, Y. Li, Z. Li, F.-L. Zhang, Y. Gu, C. Han, G. Yang and L. Qu, *Food Chem.*, 2022, **381**, 132208.

111 N. H. Ly, T. H. Nguyen, N. Đ. Nghi, Y.-H. Kim and S.-W. Joo, *Sensors*, 2019, **19**, 1355.

112 J. Chen, M. Huang, L. Kong and M. Lin, *Carbohydr. Polym.*, 2019, **205**, 596–600.

113 M. J. S Oliveira, I. Bianchi-Carvalho, R. J. G Rubira, S. Sánchez-Cortés and C. J. L Constantino, *ACS Omega*, 2024, **9**, 42571–42581.

114 Z. Chen, R. Tan, M. Zeng, X. Yuan, K. Zhuang, C. Feng, Y. He and X. Luo, *Food Chem.*, 2024, **439**, 138110.

115 L. Carles, H. Gardon, L. Joseph, J. Sanchís, M. Farré and J. Artigas, *Environ. Int.*, 2019, **124**, 284–293.

116 L. S. Murcia-Correa, O. C. Usuriaga, L. Vieira and L. Raniero, *Sens. Actuators, B*, 2023, **302**, 123017.

117 G. Emonds-Alt, C. Malherbe, A. Kasemiire, H. T. Avohou, P. Hubert, E. Ziemons, J.-C. M. Monbaliu and G. Eppe, *Talanta*, 2022, **249**, 123640.

118 E. Yavuz, M. Sakir, M. S. Onses, S. Salem and E. Yilmaz, *Talanta*, 2024, **279**, 126640.

119 X. Jin, J. Huang, H. Zhang, M. Wang, D. Xie and W. Jia, *Sens. Actuators, B*, 2025, **334**, 125881.

120 X. Tu, J. Yuan, S. Xu and X. Zhang, *J. Hazard. Mater.*, 2025, **482**, 136519.

121 C. Ye, M. He, Z. Zhu, X. Shi, M. Zhang, Z. Bao, Y. Huang, C. Jiang, J. Li and Y. Wu, *J. Mater. Chem. C*, 2022, **10**, 12966–12974.

122 H. Lai, H. Dai, G. Li and Z. Zhang, *Sens. Actuators, B*, 2022, **369**, 132360.

123 X. Wang, X. Zhu, Y. Tao, E. Zhang and X. Ren, *Sens. Actuators, B*, 2023, **290**, 122277.

124 S. Ji, S. Kou, M. Wang, H. Qiu, X. Sun, J. Dou and Z. Yang, *Appl. Surf. Sci.*, 2019, **489**, 1002–1009.

125 H. Fang, X. Zhang, S. J. Zhang, L. Liu, Y. M. Zhao and H. J. Xu, *Sens. Actuators, B*, 2015, **213**, 452–456.

126 H. Tang, D. Fang, Q. Li, P. Cao, J. Geng, T. Sui, X. Wang, J. Iqbal and Y. Du, *J. Food Sci.*, 2012, **77**, T105–T109.

127 J. Chen, Y. Huang, P. Kannan, L. Zhang, Z. Lin, J. Zhang, T. Chen and L. Guo, *Anal. Chem.*, 2016, **88**, 2149–2155.

128 M. M. Hassan, M. Zareef, T. Jiao, S. Liu, Y. Xu, A. Viswadevarayalu, H. Li and Q. Chen, *Food Chem.*, 2021, **338**, 127796.

129 T. Mu, S. Wang, T. Li, B. Wang, X. Ma, B. Huang, L. Zhu and J. Guo, *IEEE J. Sel. Top. Quantum Electron.*, 2019, **25**, 1–6.

130 N. Chamuah, N. Bhuyan, P. P. Das, N. Ojah, A. J. Choudhary, T. Medhi and P. Nath, *Sens. Actuators, B*, 2018, **273**, 710–717.

131 G. Shi, M. Wang, Y. Zhu, Y. Wang and W. Ma, *Opt. Commun.*, 2018, **425**, 49–57.

132 T. Gong, Y. Huang, Z. Wei, W. Huang, X. Wei and X. Zhang, *Nanotechnology*, 2020, **31**, 205501.

133 D. Li, G. Zheng, H. Jia and J. Wang, *Colloids Surf., A*, 2014, **451**, 48–55.

134 A. Mohsennezhad, H. Aminsaremi, L. Zeinalizad, V. Eskandari and H. Sahbafar, *Plasmonics*, 2024, **20**, 45–53.

135 L. Ma, E. Han, L. Yin, Q. Xu, C. Zou, J. Bai, W. Wu and J. Cai, *Food Control*, 2023, **153**, 109951.

136 M. Lv, H. Pu and D.-W. Sun, *Sens. Actuators, B*, 2024, **316**, 124336.

137 J. Pu, W. Tian, W. Shang, Y. Zhang, G. Ma and F. Xu, *Sens. Actuators, B*, 2024, **419**, 136457.

138 J. Zhou, W. Gao, J. Wu, Z. Xiang, J. Zeng, B. Wang and J. Xu, *Int. J. Biol. Macromol.*, 2024, **282**, 137115.

139 M. Lv, H. Pu and D.-W. Sun, *Food Chem.*, 2024, **433**, 137389.

140 X. Liu, W. Deng, Y. Yang, J. Xi, S. Li, L. Zhang, P. Li and W. Wu, *Int. J. Biol. Macromol.*, 2024, **282**, 137171.

141 S. S. B. Moram, C. Byram and V. R. Soma, *RSC Adv.*, 2023, **13**, 2620–2630.

142 J. Zhou, W. Gao, H. Jiang, Z. Xiang, J. Li, D. Cao, J. Zeng, B. Wang and J. Xu, *J. Agric. Food Chem.*, 2025, **73**, 8026–8039.

143 Z. Liu, Y. Wang, R. Deng, L. Yang, S. Yu, S. Xu and W. Xu, *ACS Appl. Mater. Interfaces*, 2016, **8**, 14160–14168.

144 Y. Çelik, B. Akçıl and E. Aksoy, *Fullerenes, Nanotubes Carbon Nanostruct.*, 2023, **31**, 833–844.

145 C. Zhu, X. Wang, X. Shi, F. Yang, G. Meng, Q. Xiong, Y. Ke, H. Wang, Y. Lu and N. Wu, *ACS Appl. Mater. Interfaces*, 2017, **9**, 39618–39625.

146 T. M. Daniels, P. Sreearunothai, D. Phokharatkul, A. Jomphoak, T. Pogfay and N. Nuntawong, *Nano-Struct. Nano-Objects*, 2023, **33**, 100930.

147 R. Goodrum, H. Weldekidan, H. Li, A. K. Mohanty and M. Misra, *Adv. Ind. Eng. Polym. Res.*, 2024, **7**, 37–53.

148 W. Wu, J. C. Ranasinghe, A. Chatterjee and S. Huang, *Mater. Chem. Phys.*, 2024, **318**, 129281.

149 L. Xin, Y. Liu, L. Wang and Z. Li, *J. Mater. Sci.*, 2025, **60**, 4559–4592.

150 K.-C. Hsu and D.-H. Chen, *ACS Appl. Mater. Interfaces*, 2015, **7**, 27571–27579.

151 P. Butmee, A. Samphao and G. Tumcharern, *J. Hazard. Mater.*, 2022, **437**, 129344.

152 L. Xie, X. Ling, Y. Fang, J. Zhang and Z. Liu, *J. Am. Chem. Soc.*, 2009, **131**, 9890–9891.

153 Q. Zhou, M. Jin, W. Wu, L. Fu, C. Yin and H. Karimi-Maleh, *Chemosensors*, 2022, **10**, 317.

154 J. Shi, C. Chan, Y. Pang, W. Ye, F. Tian, J. Lyu, Y. Zhang and M. Yang, *Biosens. Bioelectron.*, 2015, **67**, 595–600.

155 H. Sun, H. Liu and Y. Wu, *Appl. Surf. Sci.*, 2017, **416**, 704–709.

156 S. Atta, T. Sharaf and T. Vo-Dinh, *ACS Appl. Nano Mater.*, 2024, **7**, 11518–11529.

157 Y. Song, Y. Zhang, Y. Huang, Y. Fan and K. Lai, *Anal. Lett.*, 2020, **53**, 1003–1018.

158 X. Wang, C. Zhu, X. Hu, Q. Xu, H. Zhao, G. Meng and Y. Lei, *Appl. Surf. Sci.*, 2019, **486**, 405–410.

159 T. H. D. Nguyen, Z. Zhang, A. Mustapha, H. Li and M. Lin, *J. Agric. Food Chem.*, 2014, **62**, 10445–10451.

160 L. Zhang, C. Jiang and Z. Zhang, *Nanoscale*, 2013, **5**, 3773.

161 C. Zhu, Q. Zhao, X. Wang, Z. Li and X. Hu, *Microchem. J.*, 2021, **165**, 106090.

162 J. Yu, Y. Ma, C. Yang, H. Zhang, L. Liu, J. Su and Y. Gao, *Sens. Actuators, B*, 2018, **254**, 182–188.

163 J. He, X. Li and J. Li, *J. Environ. Chem. Eng.*, 2022, **10**, 108278.

164 J. Zhang, J. Wu, B. Wang, Y. Geng and Z. Wang, *Sens. Actuators, B*, 2024, **410**, 135711.

165 J. Wang, Y. Feng, H. Zhang, L. Han, J. Xia and G. Wang, *Sens. Actuators, B*, 2025, **329**, 125535.

166 J. Dong, X. Zhao, E. Cao, Q. Han, L. Liu, W. Zhang, W. Gao, J. Shi, Z. Zheng, D. Han and M. Sun, *Mater. Today Nano*, 2020, **9**, 100067.

167 H. Sun, S. Xiong, B. Shi, Y. Zhou, C. Bi, J. Li, L. Li, B. Liu, C. Dai, Y. Wang, C. Wang, D. Wang and W. Liu, *Colloids Surf., A*, 2024, **700**, 134647.

168 M. Yu, C. Qin, Z. Yu, B. Sun, D. Ni, D. Zhang and P. Liang, *Chemosensors*, 2024, **12**, 82.

169 L. Fabris, *J. Opt.*, 2015, **17**, 114002.

170 N. Kamkrua, T. Ngernsutivorakul, S. Limwichean, P. Eiamchai, C. Chananonnawathorn, V. Pattanasetthakul, R. Ricco, K. Choowongkomon, M. Horprathum, N. Nuntawong, T. Bora and R. Botta, *ACS Appl. Nano Mater.*, 2023, **6**, 1072–1082.

171 H. Zhao, X. Cui, P. Zhang, M. Zhou, C. Liu, X. Shi and J. Ma, *Appl. Spectrosc.*, 2024, **78**, 851–862.

172 T. Wan, L. Zhu, Z. Zhang, H. Wang, Y. Yang, H. Ye, H. Wang, L. Li and J. Li, *New J. Chem.*, 2022, **46**, 14177–14185.

173 E. Lenzi, D. Jimenez de Aberasturi and L. M. Liz-Marzán, *ACS Sens.*, 2019, **4**, 1126–1137.

174 M. Zhang, X. Li, J. Pan, Y. Zhang, L. Zhang, C. Wang, X. Yan, X. Liu and G. Lu, *Biosens. Bioelectron.*, 2021, **190**, 113421.

175 W. M. Pazin, L. N. Furini, D. C. Braz, M. Popolin-Neto, J. D. Fernandes, C. J. Leopoldo Constantino and O. N. Oliveira, *ACS Appl. Nano Mater.*, 2024, **7**, 2335–2342.

176 X. Liu, J. Guo, Y. Li, B. Wang, S. Yang, W. Chen, X. Wu, J. Guo and X. Ma, *J. Mater. Chem. B*, 2021, **9**, 8378–8388.

177 Y. Sun, N. Zhang, C. Han, Z. Chen, X. Zhai, Z. Li, K. Zheng, J. Zhu, X. Wang, X. Zou, X. Huang and J. Shi, *Food Chem.*, 2021, **358**, 129898.

178 Y. Sun, Z. Li, X. Huang, D. Zhang, X. Zou, J. Shi, X. Zhai, C. Jiang, X. Wei and T. Liu, *Biosens. Bioelectron.*, 2019, **145**, 111672.

179 H. Wang, Z. Chen, C. Zhu, H. Du, J. Mao, H. Qin, Y. She and M. Yan, *Anal. Chim. Acta*, 2023, **1268**, 341398.

180 S. Pang, T. P. Labuza and L. He, *Analyst*, 2014, **139**, 1895–1901.

181 S. Xu, M. Li, X. Li, Y. Jiang, L. Yu, Y. Zhao, L. Wen and Q. Xue, *Anal. Bioanal. Chem.*, 2023, **415**, 203–210.

182 Y. Shu, J. Li, H. Bai, A. Liang, G. Wen and Z. Jiang, *Talanta*, 2024, **267**, 125166.

183 X. Yang, Q. Liu, L. Luo, W. Tian, C. Kang, W. Yang, T. Li, D. Chen and X. Yan, *Anal. Bioanal. Chem.*, 2025, **417**, 4407–4418.

184 Y. Jiang, D.-W. Sun, H. Pu and Q. Wei, *J. Food Meas. Charact.*, 2020, **14**, 3184–3193.

185 G. B. L. Silva, L. A. C. Alvarez, F. V Campos, M. C. C. Guimar and P. Oliveira, 2024, **199**, 109952.

186 M. D. L. Jara, L. A. C. Alvarez, F. V. Campos, P. W. P. Antunes, M. C. C. Guimarães and J. P. de Oliveira, *Food Anal. Methods*, 2024, **17**, 284–295.

187 L. A. Contreras Alvarez, M. D. Lazo Jara, F. V. Campos, J. P. de Oliveira and M. C. C. Guimarães, *Food Addit. Contam.,:Part A*, 2024, **41**, 424–437.

188 X. Li, T. Yang, Y. Song, J. Zhu, D. Wang and W. Li, *Sens. Actuators, B*, 2019, **283**, 230–238.

189 E. Sheng, Y. Lu, Y. Xiao, Z. Li, H. Wang and Z. Dai, *Biosens. Bioelectron.*, 2021, **181**, 113149.

190 S. Dong, Q. Shi, Z. Zhu, J. Wu and J. Feng, *Colloids Surf., A*, 2024, **692**, 133978.

191 M. Wang, J. Feng, J. Ding, J. Xiao, D. Liu, Y. Lu, Y. Liu and X. Gao, *Chem. Eng. J.*, 2024, **487**, 150666.

192 X. Li, H. Qian, J. Tao, M. Cao, M. Wang and W. Zhai, *Nanomaterials*, 2024, **14**, 1046.

193 J. Pei, Y. Jin, C. Ren, Y. Chen, M. Zou and X. Qi, *Anal. Methods*, 2024, **16**, 3938–3948.

194 L. Ma, X. Yang, L. Yin, E. Han, C. Wang, R. Zhou, J. Bai, Y. Wang, Z. Guo and J. Cai, *J. Food Compos. Anal.*, 2024, **136**, 106781.

195 K. V. Serebrennikova, N. S. Komova, L. V. Barshevskaya, A. V. Zherdev and B. B. Dzantiev, *Microchim. Acta*, 2024, **191**, 749.

196 K. Nehra, S. K. Pandian, M. S. S. Bharati and V. R. Soma, *New J. Chem.*, 2019, **43**, 3835–3847.

197 F. Benz, R. Chikkaraddy, A. Salmon, H. Ohadi, B. de Nijs, J. Mertens, C. Carnegie, R. W. Bowman and J. J. Baumberg, *J. Phys. Chem. Lett.*, 2016, **7**, 2264–2269.

198 P. Guo, D. Sikdar, X. Huang, K. J. Si, W. Xiong, S. Gong, L. W. Yap, M. Premaratne and W. Cheng, *Nanoscale*, 2015, **7**, 2862–2868.

199 H. Guo, S. Zhi, Z. Zhao, T. Gao, H. Ma, S.-H. Luo, W. Zhang, P. Guo, B. Ren, Z.-Q. Tian and G.-K. Liu, *ACS Appl. Mater. Interfaces*, 2025, **17**, 33318–33339.

200 H. Lai, Z. Yu, G. Li and Z. Zhang, *J. Chromatogr. A*, 2022, **1675**, 463181.

201 Z. Wang, S. Zong, L. Wu, D. Zhu and Y. Cui, *Chem. Rev.*, 2017, **117**, 7910–7963.

202 H. K. Lee, Y. H. Lee, C. S. L. Koh, G. C. Phan-Quang, X. Han, C. L. Lay, H. Y. F. Sim, Y.-C. Kao, Q. An and X. Y. Ling, *Chem. Soc. Rev.*, 2019, **48**, 731–756.

203 M.-L. Xu, Y. Gao, X. X. Han and B. Zhao, *J. Agric. Food Chem.*, 2017, **65**, 6719–6726.

204 M. Ortiz-Martínez, J. A. Molina González, G. Ramírez García, A. Luna Bugallo, M. A. Justo Guerrero and E. C. Strupiechonski, *Environ. Toxicol. Chem.*, 2024, **43**, 1468–1484.

205 *Metrohm, Gold P-SERS Substrate (Au), 25 pieces*, https://www.metrohm.com/pt_br/products/6/0750/607506170.html.

206 *Stellarnet, SERS Substrate Strips, 25 pieces*, https://www.stellarnet.us/spectrometers-accessories/sers-substrates/.

207 Simelco, *SERS Substrates – SERStrate*, https://www.silmeco.com/products/sers-substrate-serstrate/.

208 Oceanoptics, *Sampling Accessories, SERS substrate*, https://www.oceanoptics.com/accessories/sampling-accessories/.

209 X. Bi, L. Lin, Z. Chen and J. Ye, *Small Methods*, 2023, **8**(1), DOI: 10.1002/smtd.202301243.

210 J. Yi, E.-M. You, G.-K. Liu and Z.-Q. Tian, *Nat. Nanotechnol.*, 2024, **19**, 1758–1762.

211 M. Zarei, N. V. Solomatova, H. Aghaei, A. Rothwell, J. Wiens, L. Melo, T. G. Good, S. Shokatian and E. Grant, *Anal. Chem.*, 2023, **95**, 15908–15916.

212 X. Bi, X. Ai, Z. Wu, L. L. Lin, Z. Chen and J. Ye, *Anal. Chem.*, 2025, **97**, 6826–6846.